Search For Right Handed Currents in Leptonic Tau Decays

by

Kevin Graham
H.B.Sc., University of Western Ontario, 1992

A Dissertation Submitted in Partial Fulfillment of the
Requirements for the Degree of

MASTERS OF SCIENCE

in the Department of Physics and Astronomy

We accept this thesis as conforming
to the required standard

[redacted]

Dr. R.K. Keeler, Co-supervisor (Department of Physics and Astronomy)

[redacted]

Dr. R. Sobie, Co-supervisor (Department of Physics and Astronomy)

[redacted]

Dr. G. Beer, Departmental Member (Department of Physics and Astronomy)

[redacted]

Dr. M. Roney, External Member (Department of Physics and Astronomy)

[redacted]

Dr. T. Gough, Outside Member (Department of Chemistry)

[redacted]

Dr. D. Axen, External Examiner (University of British Columbia)

Co-supervisors: Dr. R. K. Keeler and Dr. R. Sobie

ABSTRACT

The form of the coupling for the charged weak current is assumed to be V-A in the Standard Model. This structure has been well tested in muon decays but there have only been a small number of such tests in leptonic tau decays. This thesis uses data collected by the OPAL experiment at LEP to determine the ξ Michel parameter for leptonic tau decays: $\xi = 0.79^{+0.28}_{-0.44}$. This is consistent with the pure V-A prediction of the Standard Model.

Examiners:

[redacted]

Dr. R.K. Keeler, Co-supervisor (Department of Physics and Astronomy)

[redacted]

Dr. R. Sobie, Co-supervisor (Department of Physics and Astronomy)

[redacted]

Dr. G. Beer, Departmental Member (Department of Physics and Astronomy)

[redacted]

Dr. M. Roney, External Member (Department of Physics and Astronomy)

[redacted]

Dr. T. Gough, Outside Member (Department of Chemistry)

[redacted]

Dr. D. Axen, External Examiner (University of British Columbia)

Contents

List of Tables

List of Figures

Chapter 1

Introduction

All measurements to date indicate that weak interactions can be described in terms of purely left handed currents. The research described here examines the nature of the weak interaction structure for leptonic tau decays. A theoretical model that includes right handed currents is introduced and the measurement of a parameter ξ which characterises the handedness of an interaction is presented.

1.1 Historical Overview

The study of the weak interaction began with measurements of nuclear beta decay. By the 1930's it was recognised that many atoms were unstable and decayed into lighter elements by electron emission. Only two particles, the new atom and an electron, were observed in these processes. Experimental measurements [1] revealed that electrons from beta decay were not mono-energetic as expected for a two body decay but exhibited a continuous energy spectrum.

Pauli proposed that an undetected third particle called a neutrino (ν) was involved [2]. In 1934 Fermi constructed a theoretical model based on Pauli's idea that agreed with experiment [3]. Fermi's interaction Lagrangian took the form of the four particle contact interaction

$$\mathcal{L} = -C_V(\overline{\Psi}_p\gamma_\mu\Psi_n)(\overline{\Psi}_e\gamma^\mu\Psi_\nu). \tag{1.1}$$

The four Ψ's are the proton, neutron, electron and neutrino wave functions respectively. C_V is the interaction coupling constant and the γ_μ's are Dirac matrices. The structures

$\overline{\Psi}\Gamma\Psi$ are referred to as Dirac currents in analogy to electromagnetic currents. The Dirac currents in 1.1 are called vector currents because they transform like polar vectors under parity transformations (spatial inversion) and are Lorentz invariant four vectors. There are five possible current types. Each type is denoted by its parity transformation properties and it's covariant Lorentz rank. The five types are: scalar, pseudo-scalar, vector, axial-vector and tensor. Gamov and Teller generalised Fermi's interaction to include all possible current forms as [4]

$$\mathcal{L} = -\sum_i C_i(\overline{\Psi}_p\Gamma_i\Psi_n)(\overline{\Psi}_e\Gamma^i\Psi_\nu) \qquad (1.2)$$

where the sum is over the Dirac matrices $\Gamma_S = 1$, $\Gamma_P = \gamma^5$, $\Gamma_V = \Gamma^\mu$, $\Gamma_A = \gamma^\mu\gamma^5$ and $\Gamma_T = \sigma^{\mu\nu}$. By the middle of the 1950's, no conclusive evidence had been produced to fix the coupling constants in 1.2.

In the meantime, several other developments in particle physics had occurred. Anderson's discovery of the positron [5] in 1932 had given surprising evidence in favour of Dirac's relativistic equation for free electrons. This supported the theory that all particles in nature have corresponding antiparticles. In 1937 Street and Stevenson [6] and, independently, Neddermeyer and Anderson [7] discovered a new charged particle from cosmic ray experiments. Except for it's large mass, the new particle appeared to be identical to the electron and was eventually called the muon (μ) [8] [9].

Lattes *et al.* [10] discovered that the source of cosmic ray muons was the decay of π mesons (or pions). In addition, their experiments clearly suggested that an unobserved particle was involved in the decay. Observations showed that the generated muon energies were consistent with a two body pion decay $\pi^- \rightarrow \mu^-\overline{\nu}_\mu$. It was supposed that the unknown particle may be the same particle that was involved in beta decay.

Examination of muon decays to electrons also indicated the presence of undetected particles. However, the decays produced a continuous spectrum of electron energies like beta decay [11]. It appeared that muon decay was also a three body decay $\mu^- \rightarrow e^-\overline{\nu}_e\nu_\mu$ that included two of the neutrino particles.

In 1953 Reines and Cowan [12] conclusively proved the existence of the mysterious neutrino. Using the flux of neutrinos from a nuclear reactor they were able to measure

positron production from the reaction

$$\overline{\nu}_e + p^+ \longrightarrow n + e^+. \tag{1.3}$$

By the end of the 1950's Davis *et al.* [13] had shown that the neutrino in reaction 1.3 was actually an antineutrino ($\overline{\nu}$) and that this was distinct from the neutrino that appears in

$$\nu_e + n \longrightarrow p^+ + e^-. \tag{1.4}$$

This lead to the discovery in 1962 of the muon neutrino by Danby *et al.* [14]. After carefully extracting muon neutrinos from pion decay they observed the creation of muons but no electrons from

$$\overline{\nu}_\mu + p^+ \longrightarrow n + \mu^+. \tag{1.5}$$

This evidence along with the apparent forbidden nature of the muon decay $\mu \rightarrow e + \gamma$ [15] suggested that electrons and muons were different in some fundamental way other than their mass. The family of particles including the electron, muon and the neutrinos is known as the leptons. These particles only interact via the weak force or, for the charged members, through the electromagnetic force. The electron and its neutrino form what is called the first generation while the muon and its neutrino form the second generation.

Until 1956 physicists believed that parity was conserved in all interactions. Experimentalists had discovered two particles that appeared identical except that the first decayed into two pions while the second decayed into three pions. Noting that the two final states have opposite total parity, Lee and Yang [16] proposed that the two particles were really the same particle. The opposite parity final states could be interpreted by assuming that parity was not conserved in one of the decays. The following year Wu *et al.* [17] proved that parity was violated in the beta decay of ^{60}Co nuclei confirming that the weak interaction was a parity violating one.

Returning to 1.2 and incorporating parity violation gives a general Lagrangian of the form

$$\mathcal{L} = -\sum_i (\overline{\Psi}_p \Gamma_i \Psi_n)(\overline{\Psi}_e \Gamma^i (C_i + C_i' \gamma^5) \Psi_\nu). \tag{1.6}$$

A parity transformation changes the relative sign on the C_i' term with respect to C_i. Thus a non-zero measurement of C_i' indicates parity violation. Numerous measurements were conducted using beta decays and resulted in constraints on the coupling constants in 1.6 that correspond to the matrix element

$$\mathcal{M} = C_V(\overline{\Psi}_p\gamma_\mu(1 - 1.26\gamma^5)\Psi_n)(\overline{\Psi}_e\gamma^\mu(1 - \gamma^5)\Psi_\nu). \tag{1.7}$$

The electron-neutrino current is called V-A because it exhibits the form (vector)-(axial-vector). It is referred to as a charged current because it involves the exchange of charge. The proton-neutron current does not appear exactly as V-A because it does not represent an interaction between fundamental (point-like) particles. If the interaction were modelled at the quark level it is expected to be exactly V-A since, at present, quarks are believed to be point-like objects. The charged weak interaction is said to violate parity maximally because the vector and axial-vector contributions appear with equal coefficients.

Any Dirac wavefunction may be decomposed into left and right handed components. The notion of handedness, or chirality, is related to helicity. Helicity is defined as the projection of spin along the direction of particle momentum and is ± 1 for a spin $\frac{1}{2}$ particle in a definite helicity state. Massless spin $\frac{1}{2}$ particles travel at the speed of light and must exist in a definite helicity state. In general, massive spin $\frac{1}{2}$ particles are not in a definite helicity state but are very nearly so in the relativistic limit. The V-A structure of charged weak currents is equivalent to selecting left handed particles. This implies that only left handed massless spin $\frac{1}{2}$ (helicity -1) particles will interact weakly. In particular, a massless neutrino is always left handed. For antiparticles the structure is reversed. The charged weak interaction is always V+A and a massless antineutrino is always right handed.

During the 1960's many researchers focused their attention on muon decay. The structure of the weak force in this interaction was closely examined to determine if it corresponded to the results from beta decay. Many precision tests showed that experimental data was consistent with a V-A structure. [4] [18] [19].

At the same time, advances in the theoretical understanding of weak processes was leading to fundamental change. Fermi had supposed that beta decay could convincingly be modelled by an interaction that took place at a single space-time point. Calculations

produced reasonable results at low energies but appeared to diverge as the interaction energy increased. In analogy to the photon propagator in electromagnetic interactions, the idea that a particle mediated the weak interaction was introduced (see figure 1.1). The short range, low energy behaviour of charged weak interactions suggested that the

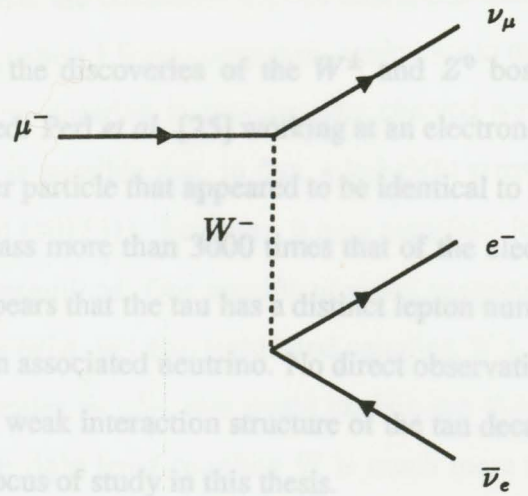

Figure 1.1: The decay of μ^- to an electron and neutrinos through the exchange of a W^-.

particle must be massive. Since the known weak interactions involved an exchange of charge it was assumed that there were two oppositely charged massive weak mediators, the $W^{\pm}$. However, this hypothesis introduced other divergences in higher order terms of the perturbative expansion used to calculate interaction cross-sections. It was shown that these difficulties could be overcome if an additional massive neutral mediator called the Z^0 was included [20]. The theoretical structure of weak interactions was combined with that of electromagnetic interactions by Glashow, Weinberg and Salam [21]. This model has become known as the Standard Model of electroweak interactions.

In 1973, Hasert *et al.* [22] proved the existence of neutral weak interactions by observing the reactions

$$\begin{aligned} \nu_\mu + N &\longrightarrow \nu_\mu + X \\ \overline{\nu}_\mu + N &\longrightarrow \overline{\nu}_\mu + X. \end{aligned} \tag{1.8}$$

This was a spectacular success for the electroweak model.

In 1983 the UA1 and UA2 experiments at CERN added another triumph for the electroweak model by discovering the W and Z particles [23] [24]. The observation of the weak interaction mediating particles led to the construction of current experiments designed specifically to create large quantities of these particles to further test the electroweak model.

A decade before the discoveries of the $W^{\pm}$ and Z^0 bosons a third generation of leptons was discovered. Perl *et al.* [25] working at an electron-positron collider at SLAC discovered yet another particle that appeared to be identical to the electron. This time the new particle had a mass more than 3000 times that of the electron and was denoted the tau particle (τ). It appears that the tau has a distinct lepton number from the electron and muon and has it's own associated neutrino. No direct observation has yet shown proof of the ν_τ existence. The weak interaction structure of the tau decay to electrons and muons $\tau^- \rightarrow \ell^- \overline{\nu}_\ell \nu_\tau$ is the focus of study in this thesis.

1.2 Current Research

The Standard Model assumes that all charged weak interactions occur via a V-A (left hand) structure. The analysis presented here attempts to search for a possible deviation from pure V-A in the form of a V+A (right hand) component in the leptonic decays of tau particles. In this case, a leptonic decay means that all of the particles involved are leptons. Specifically, the known leptonic tau decays are

$$\begin{aligned} \tau^- &\longrightarrow e^- + \overline{\nu}_e + \nu_\tau \\ \tau^- &\longrightarrow \mu^- + \overline{\nu}_\mu + \nu_\tau \end{aligned} \tag{1.9}$$

These decays are of particular interest because they appear to deal with point-like particles that only interact weakly or electromagnetically.

The first completely leptonic tests of the Standard Model charged weak interaction studied the decay of muons to electrons (figure 1.1)

$$\mu^- \longrightarrow e^- + \overline{\nu}_e + \nu_\mu. \tag{1.10}$$

Since it is extremely difficult to detect neutrinos, experiments have focused on examining the decay electrons. Measurement of the energy and angular distributions of these electrons provides information about the structure of the charged weak currents in muon decay. Specifically, the shape of the spectrum is different for V-A and V+A interactions. All of the experiments to date are consistent with an interaction that is V-A [26] [27] [28] [29]. The tau decays in equation 1.9 are completely analogous to the muon decay.

It is an interesting question to wonder why charged weak interactions seem to be only left handed. It is possible that, in fact, a left-right symmetry does exist in charged weak interactions [4] [30] [31]. However, it only manifests itself at energies higher than have currently been examined. One specific proposal suggests that, not only do left hand coupling W particles exist, but also right hand coupling W's. Since the Standard Model muon decay width scales as $\frac{1}{M_W^4}$, one might explain the V-A dominance at low energy by assuming that the right hand coupling W is much more massive than the left hand one. Muon decay experiments have placed limits on a right hand coupling W mass of $M_{W_R} > 432$ GeV [28].

The charged weak structure of leptonic tau decays has not yet been examined as thoroughly as it has for muon decays. It is possible that the three lepton generations may have different interactions. In particular, limits on a V+A contribution as described above have only been examined by the ARGUS [32] [33] and ALEPH [34] experiments. We will examine the energy spectrum of electrons and muons from tau decays produced at LEP in an attempt to place a limit on a V+A contribution.

The tau particles studied in this thesis are created at the LEP collider through electron-positron annihilation. There is a large resonance for $e^+e^- \rightarrow Z^0$ at centre of mass energies equal to the mass of the Z^0 (see 1.2). The Z^0 particles decay approximately 3.4% of the time into two oppositely charged taus producing a large sample of tau leptons. The structure of this neutral weak interaction causes the produced taus to have opposite helicities and, in addition, predicts a partial polarisation of the taus.

Tau pair events are selected so that one tau has decayed to a muon and the other to an electron. Such an event would follow the sequence

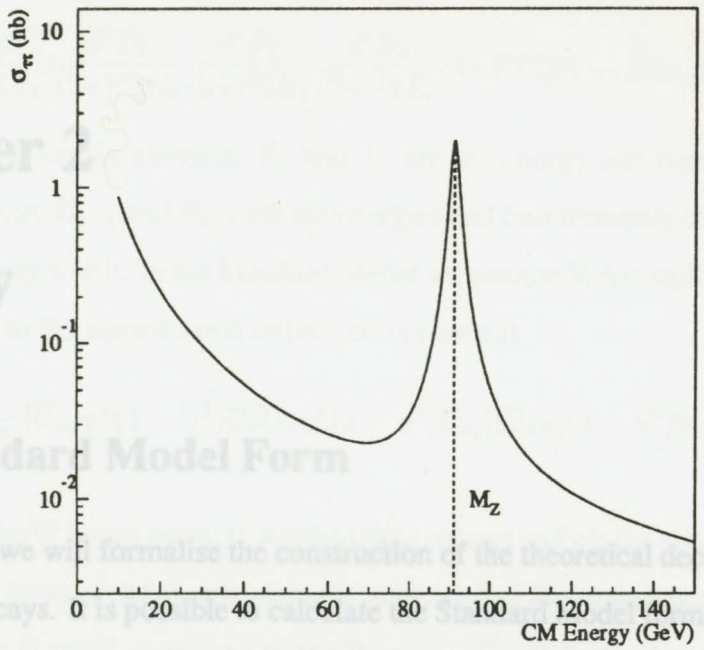

Figure 1.2: Cross section for tau pair production at the Z mass.

$$e^+e^- \rightarrow Z^0 \rightarrow \begin{cases} \tau^- \rightarrow \ell^- + \overline{\nu}_\ell + \nu_\tau \\ \tau^+ \rightarrow \ell^+ + \nu_\ell + \overline{\nu}_\tau \end{cases} \tag{1.11}$$

where $\ell^\pm$ refers to either a muon or electron. In the following work we will refer to tau pair events in which both tau particles decay to leptons as correlated leptonic tau decays.

It will be shown in Chapter 2 that the decay spectra for leptonic tau decays are sensitive to both the tau polarisation, P_τ, and the form of the coupling involved. The structure of the coupling can be characterised by the parameter ξ which, in this work, is the fractional difference between left and right handed contributions. A method is described that allows the use of correlated leptonic tau decays to determine P_τ and ξ up to a relative sign. Chapter 3 gives a description of the experimental apparatus used for the measurement. The data selection algorithms are detailed in Chapter 4. The analysis of the spectra is discussed in Chapter 5. Chapter 6 will present the results and discuss previous measurements.

Chapter 2

Theory

2.1 Standard Model Form

In this chapter we will formalise the construction of the theoretical decay distribution for leptonic tau decays. It is possible to calculate the Standard Model form of the differential decay at the tree level (i.e. lowest order). The decay is a three body decay of the form

$$\tau^- \longrightarrow \ell^- + \overline{\nu}_\ell + \nu_\tau \tag{2.1}$$

where ℓ is either an electron or a muon. The corresponding tree level Feynman diagram

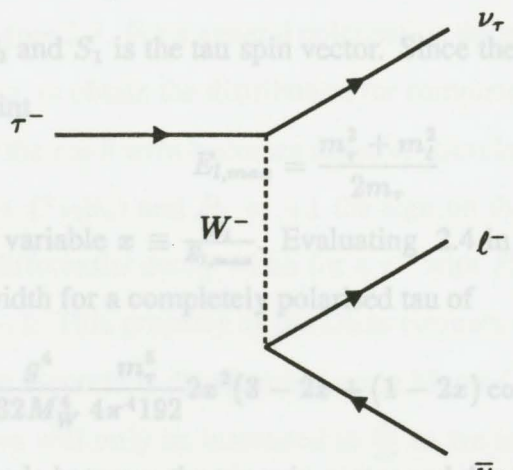

Figure 2.1: Tree level Feynman Diagram of leptonic tau decay.

may found in figure 2.1. The calculation of the tau leptonic decay distribution parallels exactly the procedure followed for muon decay.

In general, a three body differential decay has the form [4]

$$d\Gamma = \frac{|M|^2}{2E_1}\frac{d^3\boldsymbol{P_2}}{(2\pi)^3 2E_2}\frac{d^3\boldsymbol{P_3}}{(2\pi)^3 2E_3}\frac{d^3\boldsymbol{P_4}}{(2\pi)^3 2E_4}(2\pi)^4\delta^4(P_1 - P_2 - P_3 - P_4) \tag{2.2}$$

where M is the matrix element, E_1 and P_1 are the energy and four momentum of the decaying particle, E_{2-4} and P_{2-4} are the energies and four momenta of the decay products and Γ is the decay width. In the Standard Model we assume V-A coupling at the interaction points leading to the squared first order matrix element

$$|M|^2 = \frac{g^4}{64M_W^4}[\overline{U}_{\nu_\tau}\gamma^\mu(1-\gamma^5)U_\tau\overline{U}_\tau\gamma^\nu(1-\gamma^5)U_{\nu_\tau}][\overline{U}_\ell\gamma_\mu(1-\gamma^5)V_{\nu_\ell}\overline{V}_{\nu\ell}\gamma_\nu(1-\gamma^5)U_\ell] \tag{2.3}$$

where M_W is the W boson mass, U_i are the Dirac spinors and g is the charged weak coupling constant. This form of the matrix element assumes that the momentum transferred to the decay products is small compared to the W mass. The V-A structure is contained in the Dirac matrix $\gamma^\mu(1-\gamma^5)$. After summing over the final state spins in 2.3 and integrating over the undetected neutrino momenta in 2.2 we are left with

$$d\Gamma = \frac{g^4 d^3P_2}{96(2\pi)^4 E_1 E_2 M_W^4}[P^2 P_2\cdot(P_1 - m_1 S_1) + 2P\cdot P_2 P\cdot(P_1 - m_1 S_1)] \tag{2.4}$$

where $P = P_1 - P_2$ and S_1 is the tau spin vector. Since the tau is at rest we observe the kinematical constraint

$$E_{l,max} = \frac{m_\tau^2 + m_l^2}{2m_\tau} \tag{2.5}$$

and may define the variable $x \equiv \frac{E_l}{E_{l,max}}$. Evaluating 2.4 in the tau rest frame yields the differential decay width for a completely polarised tau of

$$d\Gamma = \frac{g^4}{32M_W^4}\frac{m_\tau^5}{4\pi^4 192}2x^2(3 - 2x + (1-2x)\cos\theta)dx\,d\cos\theta\,d\phi \tag{2.6}$$

where theta is the angle between the tau spin vector and the decay lepton momentum (see figure 2.2) and we have assumed the mass of the decay lepton is small compared to the mass of the tau. The polarisation is defined by

$$P_\tau = \frac{N_\uparrow - N_\downarrow}{N_\uparrow + N_\downarrow} \tag{2.7}$$

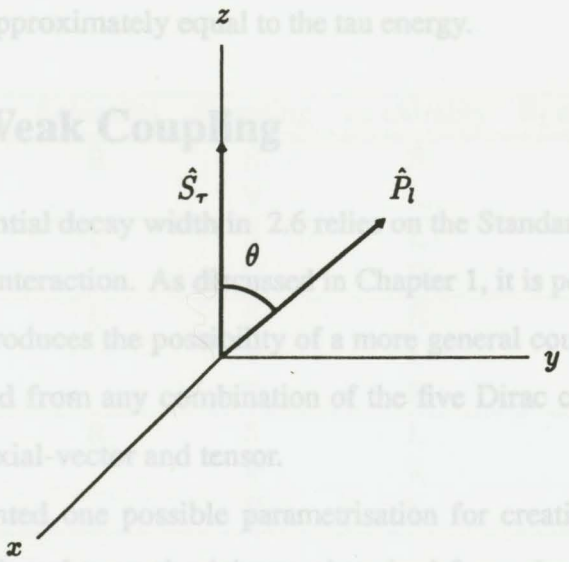

Figure 2.2: Shown is the co-ordinate system in the tau rest frame used to describe the decay of a tau with the tau spin aligned along the z axis. $\hat{S}_\tau$ is the direction of the tau spin vector, $\hat{P}_\ell$ is the direction of the decay lepton momentum and θ is the angle between $\hat{S}_\tau$ and $\hat{P}_\ell$.

where $N_\uparrow$ is the number of tau particles with spin aligned parallel to the z axis in the experimental reference frame and $N_\downarrow$ is the number with spin aligned anti-parallel to the z axis. Equation 2.6 is valid for the case when all tau spins are aligned parallel to the z axis and corresponds to figure 2.2. For a general polarisation the $\cos\theta$ term in 2.6 is multiplied by the factor P_τ. Thus, to obtain the distribution for complete polarisation anti-parallel to the z axis the sign of the $\cos\theta$ term becomes negative. Similarly, for the charge conjugate decay of 2.1 ($\tau^+ \rightarrow \ell^+\nu_\ell\overline{\nu}_\tau$) and $P_\tau = +1$ the sign on the $\cos\theta$ term again becomes negative. Thus the differential decay width for a τ^- with $P_\tau = +1$ is equivalent to that for a τ^+ with $P_\tau = -1$. This property of the Dirac currents will be exploited later in the thesis to construct the theoretical distributions using Monte Carlo events.

In this analysis we will only be interested in $\frac{d\Gamma}{dx}$ so we integrate over $d\cos\theta d\phi$. The tau particles detected by OPAL are not created at rest and hence 2.6 must be boosted to the lab frame. Equation 2.6 then becomes [35]

$$\frac{1}{\Gamma}\frac{d\Gamma}{dx} = \frac{1}{3}[5 - 9x^2 + 4x^3 + P_\tau(1 - 9x^2 + 8x^3)] \qquad (2.8)$$

and is normalised to unity. The variable x is still defined as $x \equiv \frac{E_l}{E_{l,max}}$ but since the tau

is not at rest $E_{l,max}$ is approximately equal to the tau energy.

2.2 General Weak Coupling

The form of the differential decay width in 2.6 relies on the Standard Model assumption of a strictly V-A weak interaction. As discussed in Chapter 1, it is possible to construct a matrix element that introduces the possibility of a more general coupling structure. The form can be constructed from any combination of the five Dirac current types: scalar, pseudo-scalar, vector, axial-vector and tensor.

Equation 1.6 presented one possible parametrisation for creating a general matrix element. It is often referred to as the 'charge changing' form since the Dirac currents connect particles with different charge. More recent experiments have presented a second parametrisation known as the 'chiral projection' form [18]. The chiral projection operators are defined as

$$\Lambda_L = \frac{1}{2}(1-\gamma^5)$$
$$\Lambda_R = \frac{1}{2}(1+\gamma^5). \tag{2.9}$$

Since $\Lambda_L + \Lambda_R = 1$ we may rewrite any wavefunction u as

$$u = u_L + u_R. \tag{2.10}$$

$u_L = \Lambda_L u$ is called the left handed projection of u while $u_R = \Lambda_R u$ is called the right handed projection of u. Since $\Lambda_L \Lambda_R = 0$, u_R and u_L form a linearly independent basis for the wavefunction. This means that contracting wavefunctions with opposite chirality will return a null result. Incorporating chiral projections into the parametrisation we may write the most general, local, derivative free matrix element for the decay 2.1 as

$$M = \frac{4G_F}{\sqrt{2}} \sum_{\gamma;ab} g^{\gamma}_{ab} [\overline{U}_{\nu_\tau} \Gamma^{\gamma} U^a_{\tau}][\overline{U}^b_{\ell} \Gamma_{\gamma} V_{\nu\ell}] \tag{2.11}$$

where the sum γ is over the gamma matrices 1, γ^μ and $\sigma^{\mu\nu}$ and the sums a and b are over the chiral projections of the charged lepton wavefunctions. Since the wavefunctions are

τ chirality	ℓ chirality	Coupling	ν_τ chirality	$\overline{\nu}_\ell$ chirality
R	R	S	R	L
		V	L	R
L	L	S	L	R
		V	R	L
R	L	S	R	R
		V	L	L
		T	R	R
L	R	S	L	L
		V	R	R
		T	L	L

Table 2.1: Chirality combinations for the various coupling types that lead to non-zero matrix element calculations.

chiral projections, equation 2.11 corresponds to a mixture of scalar and pseudoscalar (S) for $\gamma = 1$, a mixture of vector and axial-vector (V) for $\gamma = \gamma^\mu$ and tensor (T) for $\gamma = \sigma^{\mu\nu}$. The Standard Model form is given when $g^V_{LL} = 1$ and the other cases of g^γ_{ab} are equal to zero.

Equation 2.11 has the attractive feature that a specific selection of γ (S, V or T) will either leave a particle's chirality unchanged or will reverse it. Hence, for a given γ and for specific chiral projections of the charged leptons a, b the neutrino chiralities are determined. This is equivalent to saying that the helicity state for the neutrinos is determined since, for massless particles, a chiral projection is the same as a definite helicity state. Table 2.1 lists the wave function chiral combinations which give rise to non-trivial matrix calculations for the three choices of γ.

Equation 2.11 is modelling a contact interaction and thus the propagator nature of the weak force is neglected. The constants g^γ_{ab} are the coupling coefficient constants. When evaluating the differential decay using 2.11 it is useful to redefine the coupling constants in the form of the so called Michel parameters [37]. Evaluating in the lab frame and

$\ell - \overline{\nu}_\ell$	$\tau - \nu_\tau$	ρ	ξ	δ
V-A	V-A	3/4	1	3/4
V	V	3/8	0	0
A	A	3/8	0	0
V+A	V+A	3/4	-1	3/4
V-A	V	3/8	2	3/6
V-A	A	3/8	2	3/16
V-A	V+A	0	3	0

Table 2.2: Michel parameter values for various interaction couplings.

integrating over the angular dependence we obtain [35]

$$\frac{1}{\Gamma}\frac{d\Gamma}{dx} = 2 - 6x^2 + 4x^3 + \frac{4}{9}\rho(-1 + 9x^2 - 8x^3) \\ -\xi P_\tau[-\frac{2}{3} + 4x - 6x^2 + \frac{8}{3}x^3 + \frac{4}{9}\delta(1 - 12x + 27x^2 - 16x^3)] \quad (2.12)$$

where P_τ is the tau polarisation and ρ, ξ and δ are functions of the g^γ_{ab} constants. Note that without the angular decay information only 3 of the parameters are available for study. Equation 2.12 neglects a term of order $\frac{m_l}{m_\tau}$ which would include the additional parameter η.

2.3 Right handed currents

Previous experiments have measured the ρ parameter in tau decay to be $\rho = 0.74 \pm .04$ [36]. This limits the type of couplings allowed but, in particular, does not rule out the possibility of a V+A structure (table 2.2).

It is particularly interesting to examine the possibility that the charged weak current is composed of some combination of V-A and V+A couplings. One conceptual framework within which this may be conjectured is to suppose that not only do left hand coupling charged weak bosons exist, but also right hand coupling ones. In this context one would expect leptonic tau decays to proceed either by V-A or by V+A at both interaction points in figure 2.1. Since there is no *a priori* reason for requiring a left handed weak interaction

universe, this interpretation offers an attractive symmetry to the charged weak sector. The differential decay 2.6 scales as $1/M_W^4$ and hence a V+A contribution would imply some limit on a right handed W mass. Results from muon decays have placed excellent limits on possible V+A contributions but we cannot assume that similar results will hold for tau decays. It should be noted that this description has ignored the possibility that the W boson weak eigenstates are different from the mass eigenstates [4] [30] [31].

Returning to 2.12 and assuming equivalent weak and mass W eigenstates we set $\rho = \delta = \frac{3}{4}$ and get

$$\frac{1}{\Gamma}\frac{d\Gamma}{dx} = \frac{1}{3}[5 - 9x^2 + 4x^3 + \xi P_\tau(1 - 9x^2 + 8x^3)] \tag{2.13}$$

where ξ is now the fractional difference between left and right contributions

$$\xi = \frac{|g_{LL}^V|^2 - |g_{RR}^V|^2}{|g_{LL}^V|^2 + |g_{RR}^V|^2}. \tag{2.14}$$

It is apparent that with this single particle distribution we cannot determine both ξ and P_τ but only their product. However, at LEP we are creating simultaneous tau pairs produced from the decay of a spin 1 particle. To conserve spin angular momentum the created tau pairs must have anti-correlated helicities. In this context we may construct the two particle decay distribution [38]

$$\frac{1}{\sigma}\frac{d^2\sigma}{dx_1 dx_2} = \left[d\Gamma(x_1)_\uparrow^-, d\Gamma(x_1)_\downarrow^-\right] \begin{bmatrix} 0 & \sigma_{\uparrow\downarrow} \\ \sigma_{\downarrow\uparrow} & 0 \end{bmatrix} \begin{bmatrix} d\Gamma(x_2)_\uparrow^+ \\ d\Gamma(x_2)_\downarrow^+ \end{bmatrix} \tag{2.15}$$

where the terms such as $d\Gamma(x_1)_\uparrow^-$ are the appropriate single particle decay distributions for tau helicity +1 ($\uparrow$) or -1 ($\downarrow$) to negative(positive) lepton given in equation 2.13. The constants $\sigma_{\uparrow\downarrow}$ and $\sigma_{\downarrow\uparrow}$ refer to the number of tau pairs with relative helicty (+1,-1) and (-1,+1) respectively. We may express the polarisation as

$$P_\tau = \frac{\sigma_{\uparrow\downarrow} - \sigma_{\downarrow\uparrow}}{\sigma_{\uparrow\downarrow} + \sigma_{\downarrow\uparrow}} \tag{2.16}$$

and rewrite 2.15 as

$$\frac{1}{\sigma}\frac{d^2\sigma}{dx_1 dx_2} = a(x_1)a(x_2) + \xi^2 b(x_1)b(x_2) + \xi P_\tau(a(x_1)b(x_2) + a(x_2)b(x_1)) \tag{2.17}$$

where $a(x) = 5 - 9x^2 + 4x^3$, $b(x) = 1 - 9x^2 + 8x^3$ and $\sigma = \sigma_{\uparrow\downarrow} + \sigma_{\downarrow\uparrow}$. In this way we may use the correlated tau decays to disentangle the parameters ξ and P_τ.

Note that 2.17 assumes that the ξ parameter is the same for both the negative and positive tau decays. In the event that both taus decay to the same lepton type (both electron or both muon) this implies charge symmetry with respect to the weak interaction. For the case where one tau decays to an electron and the other to a muon, this assumption implies that the weak coupling of electrons to taus is the same as that for muons to taus. In this analysis symmetry with respect to charge and decay lepton type will be assumed.

2.4 Radiative Corrections

The previous discussions have been based on the decay distributions derived from the diagram in figure 2.1. This is only the lowest order estimate and to obtain a better theoretical approximation we must consider higher order diagrams. The radiative electromagnetic corrections for the process 2.1 have been calculated to order α by Kinoshita and Sirlin [39]. For the case of a mixture of V-A and V+A the corrected distribution in the tau rest frame is given by

$$\frac{1}{\Gamma}d\Gamma = [3 - 2x + \frac{\alpha}{2\pi}f(x) + \xi P_\tau \cos\theta(1 - 2x + \frac{\alpha}{2\pi}g(x))]x^2 dx d\Omega \qquad (2.18)$$

where the functions $f(x)$ and $g(x)$ may be found reference [39] and α is the fine structure constant.

Additional correction factors must be included for electroweak radiative corrections associated to the electron-positron annihilation and the tau pair production. A detailed account of these corrections may be found in reference [40].

2.5 Restructuring the Theory

Equation 2.17 would be appropriate if we measured the tree level interaction. However, it is only a first order approximation to the theory and, in addition, does not include experimental correction factors. It will prove useful to rewrite 2.17 in an equivalent form

to facilitate the introduction of these correction factors. To proceed, we first wish to rewrite 2.13 in terms of the coupling constants given in 2.14. Equation 2.14 reveals that $\xi = 1$ for V-A interactions and $\xi = -1$ for V+A interactions. If we note that $P_\tau = 1$ for +1 helicity decays and $P_\tau = -1$ for -1 helicity decays and recall the effect of charge conjugation we get

$$d\Gamma^-_\uparrow = \frac{1}{|g^V_{LL}|^2 + |g^V_{RR}|^2}[|g^V_{LL}|^2 d\Gamma^-_{\uparrow L} + |g^V_{RR}|^2 d\Gamma^-_{\uparrow R}] \tag{2.19}$$

where the terms $d\Gamma^-_{\uparrow L}$ and $d\Gamma^-_{\uparrow R}$ are obtained from 2.13 by setting the appropriate ξ and P_τ values. In equation 2.19 we have introduced the additional subscript (L,R) to denote explicitly whether the decay is via V-A (L) or V+A (R). Similarly, we construct the analogous distributions

$$d\Gamma^-_\downarrow = \frac{1}{|g^V_{LL}|^2 + |g^V_{RR}|^2}[|g^V_{LL}|^2 d\Gamma^-_{\downarrow L} + |g^V_{RR}|^2 d\Gamma^-_{\downarrow R}] \tag{2.20}$$

$$d\Gamma^+_\uparrow = \frac{1}{|g^V_{LL}|^2 + |g^V_{RR}|^2}[|g^V_{LL}|^2 d\Gamma^+_{\uparrow L} + |g^V_{RR}|^2 d\Gamma^+_{\uparrow R}] \tag{2.21}$$

$$d\Gamma^+_\downarrow = \frac{1}{|g^V_{LL}|^2 + |g^V_{RR}|^2}[|g^V_{LL}|^2 d\Gamma^+_{\downarrow L} + |g^V_{RR}|^2 d\Gamma^+_{\downarrow R}]. \tag{2.22}$$

Further examination of 2.13 reveals the following equalities:

$$\begin{aligned} d\Gamma^-_{\uparrow L} &= d\Gamma^-_{\downarrow R} = d\Gamma^+_{\downarrow L} = d\Gamma^+_{\uparrow R} \\ d\Gamma^-_{\downarrow L} &= d\Gamma^-_{\uparrow R} = d\Gamma^+_{\uparrow L} = d\Gamma^+_{\downarrow R}. \end{aligned} \tag{2.23}$$

From 2.16 and 2.14 we may construct the relations

$$\begin{aligned} \sigma_{\uparrow\downarrow} &= \frac{1}{2}(1 + P_\tau)\sigma_{tot} \\ \sigma_{\downarrow\uparrow} &= \frac{1}{2}(1 - P_\tau)\sigma_{tot} \\ |g^V_{LL}|^2 &= \frac{1}{2}(1 + \xi)(|g^V_{LL}|^2 + |g^V_{RR}|^2) \\ |g^V_{RR}|^2 &= \frac{1}{2}(1 - \xi)(|g^V_{LL}|^2 + |g^V_{RR}|^2) \end{aligned} \tag{2.24}$$

where $\sigma_{tot} = \sigma_{\uparrow\downarrow} + \sigma_{\downarrow\uparrow}$. Using the four differential decays (2.19-2.22), equations 2.23 and 2.24 we recreate 2.17 in the form

$$\frac{1}{\sigma_{tot}}\frac{d^2\sigma}{dx_1 dx_2} = \frac{1}{4}[(1+2\xi P_\tau+\xi^2)d\Gamma^-_{\uparrow L}(x_1)d\Gamma^+_{\downarrow L}(x_2) + (1-2\xi P_\tau+\xi^2)d\Gamma^-_{\downarrow L}(x_1)d\Gamma^+_{\uparrow L}(x_2) + (1-\xi^2)(d\Gamma^-_{\uparrow L}(x_1)d\Gamma^+_{\uparrow L}(x_2)+d\Gamma^-_{\downarrow L}(x_1)d\Gamma^+_{\downarrow L}(x_2))]. \quad (2.25)$$

Notice that we can only determine the relative signs of ξ and P_τ from 2.25. To determine the absolute signs further information is required from other experimental analyses and this will be discussed later.

To produce 2.25 we have relied upon the equalities in 2.23. These relations may not hold once radiative corrections are applied. Examining 2.18 reveals that this is not a concern because 2.23 is still valid after first order corrections have been introduced.

The two dimensional distributions $d\Gamma^-_{\uparrow L}d\Gamma^+_{\downarrow L}$ and $d\Gamma^-_{\downarrow L}d\Gamma^+_{\uparrow L}$ represent the V-A anti-correlated helicity decays. The remaining two distributions $d\Gamma^-_{\uparrow L}d\Gamma^+_{\uparrow L}$ and $d\Gamma^-_{\downarrow L}d\Gamma^+_{\downarrow L}$ represent V+A contributions. The particular notation employed was designed to suggest that the V+A contributions may be modelled by tau pairs with the same helicity. Indeed, it is not possible to distinguish between a contribution of like helicity taus caused by a non-standard neutral current structure and the V+A charged current decay contribution conjectured by this thesis. We will exploit this idea when creating Monte Carlo events to model the theoretical distributions. We are assuming the neutral current Standard Model results are correct in this thesis.

Figure 2.3 presents each of the the two dimensional decay distributions from 2.25. These may be compared to the Monte Carlo distributions presented in Chapter 4. As will be shown in Chapter 5, equation 2.25 is now in a suitable form to apply all of the correction factors including efficiency and resolution effects.

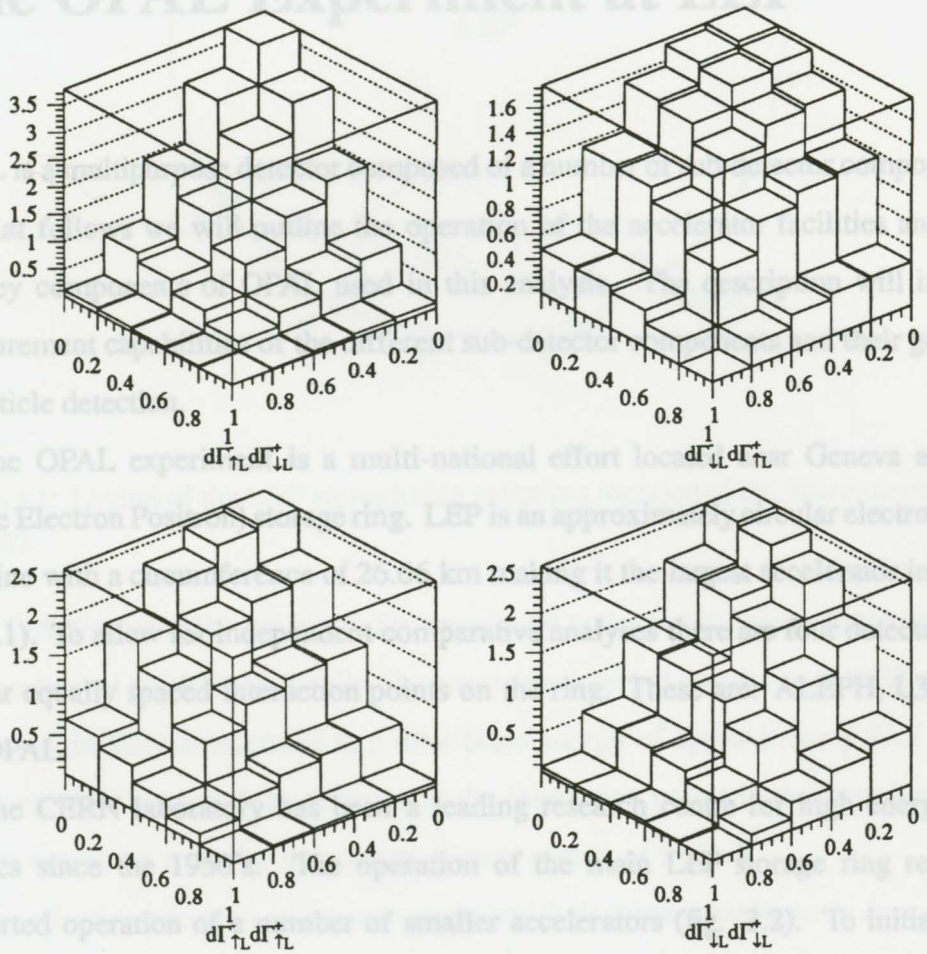

Figure 2.3: The four tree level two dimensional distributions with arbitrary scale.

Chapter 3

The OPAL Experiment at LEP

OPAL is a multipurpose detector composed of a number of sub-detector components [41]. In what follows we will outline the operation of the accelerator facilities and describe the key components of OPAL used in this analysis. The description will include the measurement capabilities of the different sub-detector components and their general role in particle detection.

The OPAL experiment is a multi-national effort located near Geneva at the LEP (Large Electron Positron) storage ring. LEP is an approximately circular electron-positron machine with a circumference of 26.66 km making it the largest accelerator in the world (fig.3.1). To allow for independent comparative analyses there are four detectors located at four equally spaced interaction points on the ring. These are: ALEPH, L3, DELPHI and OPAL.

The CERN laboratory has been a leading research centre for high energy particle physics since the 1950's. The operation of the main LEP storage ring requires the concerted operation of a number of smaller accelerators (fig. 3.2). To initiate a fill, a supply of positrons must be produced in a $e^- \rightarrow e^+$ converter. A high intensity beam of 200 MeV electrons is focused on a tungsten target to create the positrons. Electrons are generated near the converter from a low intensity gun. The positrons and electrons are then introduced into a 600 MeV linear accelerator and subsequently transferred to the 600 MeV Electron Positron Accumulation (EPA) ring. Each particle type is collected separately into 8 bunches and injected into the Proton Synchrotron (PS) where they are accelerated

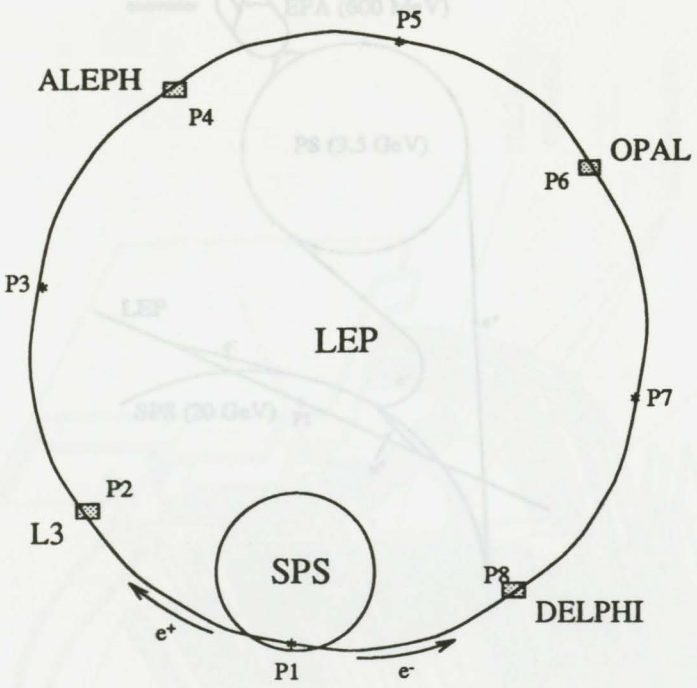

Figure 3.1: Layout of the LEP storage ring including location of the four experiments (not to scale).

to 3.5 GeV. From the PS the beams are transferred to the Super Proton Synchrotron (SPS) and accelerated to 20 GeV. Finally, the beams are injected into the main LEP ring where they are ultimately accelerated to a total beam energy of approximately 45.5 GeV. The beams are then brought into collision at the interaction points in the four detectors and physics events are recorded at a centre of mass energy of 91 GeV.

The effective selection of tau pair events and their subsequent leptonic decays requires the collection of information from all of the OPAL sub-detectors. The OPAL apparatus (fig.3.3) is an approximately cylindrical, multi-purpose magnetic spectrometer with a hermeticity of almost 98 per cent. For reference, the z coordinate is defined as parallel to the direction of the electron beam. It is then convenient to define a conventional right handed coordinate system with the inward radial direction defined as x. The detector may be roughly divided into three sections: the inner system of tracking chambers, the time-

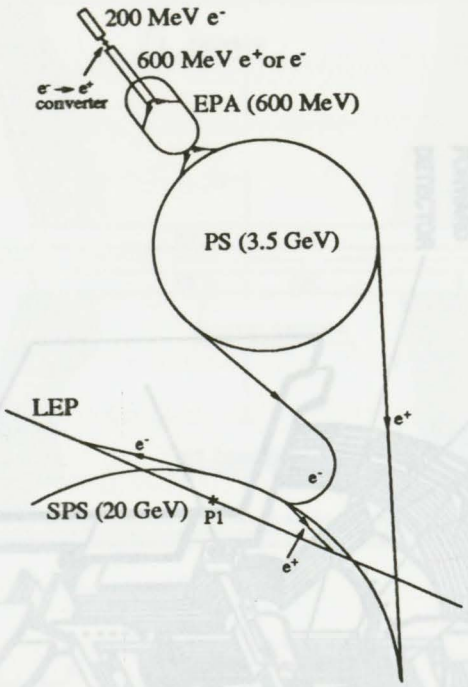

Figure 3.2: The injection system used at LEP to fill the main electron-positron storage ring (not to scale).

of-flight system and electromagnetic calorimeter in the middle section, and the hadron calorimeter and muon detectors in the outer section.

3.1 Tracking: Vertex detector, Jet Chamber and Z chambers

The central part of the OPAL detector consists of a series of drift chambers (fig.3.4) designed to track charged particles for measurements of momentum, energy loss, and primary and secondary vertex positions. To make momentum measurements and to allow charge tagging these chambers must operate in the presence of a 0.435 Tesla axial magnetic field generated by a solenoidal coil and an iron return yoke. A pressure vessel inside the magnet contains the central tracking system. The pressure vessel contains a mixture of argon, methane and isobutane (88.2, 9.8 and 2.0 per cent respectively) kept at 4 bars and which is constantly recirculated and purified.

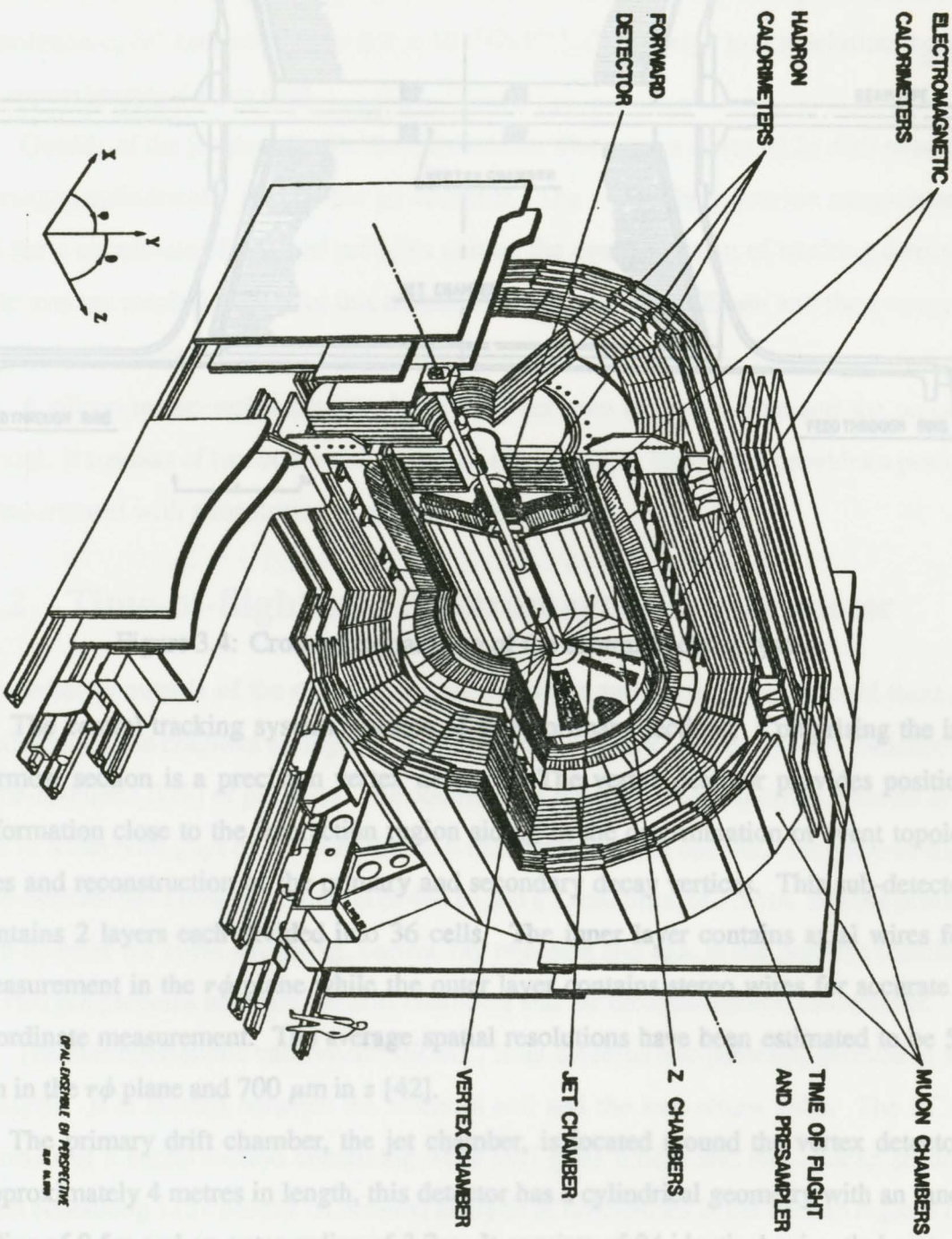

Figure 3.3: The OPAL detector at LEP. An indication of the scale is given by the figure standing at the bottom left.

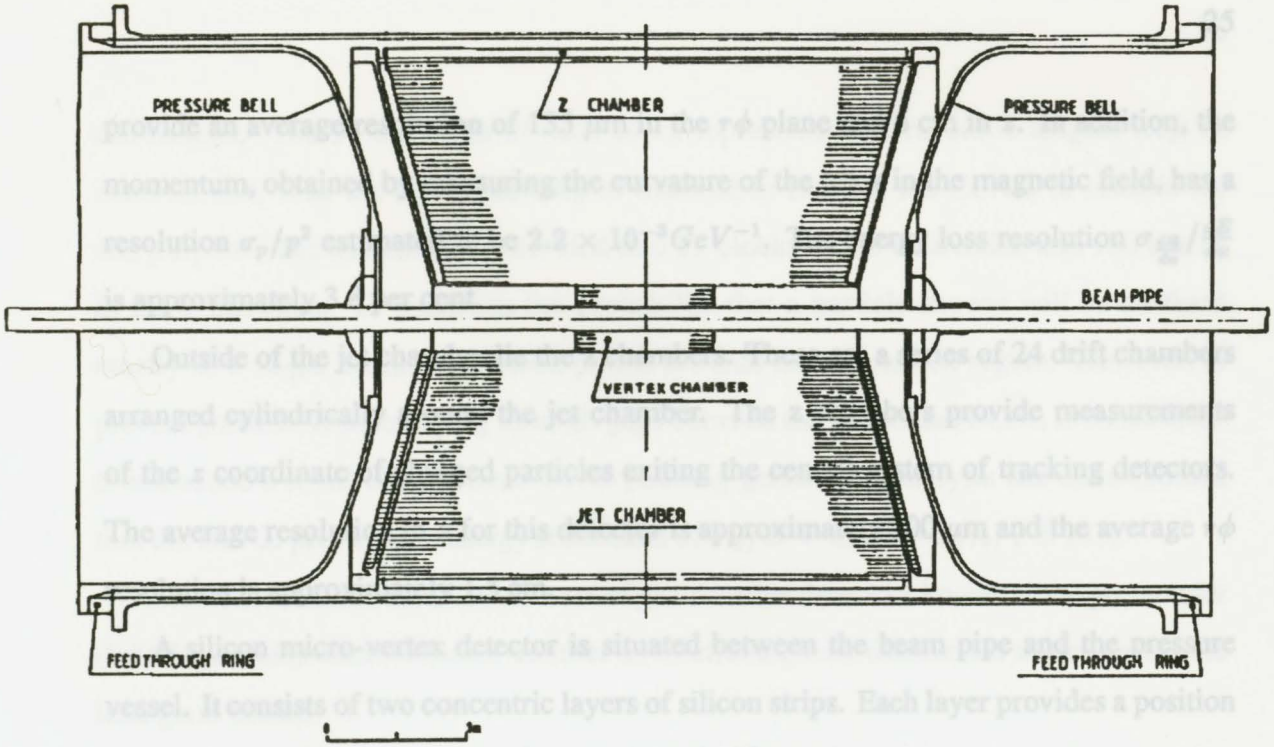

Figure 3.4: Cross sectional view of the central tracking system

The central tracking system consists of three primary sections. Comprising the innermost section is a precision vertex detector. The vertex detector provides position information close to the interaction region aiding in the determination of event topologies and reconstruction of the primary and secondary decay vertices. This sub-detector contains 2 layers each divided into 36 cells. The inner layer contains axial wires for measurement in the $r\phi$ plane while the outer layer contains stereo wires for accurate z coordinate measurement. The average spatial resolutions have been estimated to be 50 μm in the $r\phi$ plane and 700 μm in z [42].

The primary drift chamber, the jet chamber, is located around the vertex detector. Approximately 4 metres in length, this detector has a cylindrical geometry with an inner radius of 0.5m and an outer radius of 3.7m. It consists of 24 identical azimuthal sectors each containing 159 axial wires arranged in a radial plane. The jet chamber provides spatial measurements of charged particle trajectories (ie. 'tracks') and energy loss measurements used for particle identification. Position measurements have been shown to

provide an average resolution of 135 μm in the $r\phi$ plane and 6 cm in z. In addition, the momentum, obtained by measuring the curvature of the track in the magnetic field, has a resolution σ_p/p^2 estimated to be $2.2 \times 10^{-3} GeV^{-1}$. The energy loss resolution $\sigma_{\frac{dE}{dx}}/\frac{dE}{dx}$ is approximately 3.8 per cent.

Outside of the jet chamber lie the z chambers. These are a series of 24 drift chambers arranged cylindrically around the jet chamber. The z chambers provide measurements of the z coordinate of charged particles exiting the central system of tracking detectors. The average resolution in z for this detector is approximately 300 μm and the average $r\phi$ resolution is approximately 1.5 cm.

A silicon micro-vertex detector is situated between the beam pipe and the pressure vessel. It consists of two concentric layers of silicon strips. Each layer provides a position measurement with a resolution of approximately 10μm.

3.2 Time-of-flight and Electromagnetic calorimeter

Immediately outside of the central tracking chambers and the magnet solenoid there are 160 scintillation counters arranged in a cylindrical geometry. These counters measure the time-of-flight (TOF) of particles. The counters are 6.840 m long and range from 89 to 91 cm in width with gaps of no more than 2.6 mm between each counter. The time-of-flight sub-detector has a timing resolution of 460 ps and a z resolution of 7.5 cm. It is the primary sub-detector for event triggering, cosmic ray rejection and aids in the position matching of charged particles between the drift chambers and the electromagnetic calorimeter.

The electromagnetic calorimeter (ECAL) is an essential sub-detector involved in this analysis. It is located between the solenoid coil and the iron return yoke. The ECAL consists of a barrel section containing 9440 lead glass blocks and two endcap sections each containing 1132 blocks. A detailed analysis of efficiencies in the endcap regions has not been carried out and hence this analysis is confined to the barrel region.

The ECAL barrel covers an azimuthal angle of $|\cos\theta| < 0.82$ and has an inner radius of 2455 mm. The central design principle requires the ECAL detector to completely absorb electrons and photons while allowing muons and many hadrons to reach the hadronic

calorimeter. The 37 cm depth of each block represents 24.6 radiation lengths (X_0) of material and, with the additional $2X_0$ of material in front of the ECAL, is suitable for this purpose. The calorimeter is divided into 59 blocks in the z direction and 160 blocks in the ϕ direction. To maximise the probability that a particle shower will be confined mostly to a single block, each block points towards the interaction region. However, to prevent particles from escaping through gaps between the blocks the ECAL is constructed to introduce a small offset from a direct pointing geometry. Analysis has demonstrated that the ECAL provides an energy resolution of $\sigma_E/E = 1.8\% + 23\%/\sqrt{E}$ [43].

Situated in front of the ECAL is a set of gas chamber detectors known as the presampler (PB). It provides information on whether an electromagnetic shower has started before the lead glass blocks.

3.3 Hadronic Calorimeter and Muon Chambers

Surrounding the ECAL lies the iron return yoke of the magnet. The return yoke has been instrumented as a hadronic calorimeter (HCAL) to allow for hadronic shower energy measurement and muon tracking between the ECAL and the muon chambers. The HCAL consists of 9 layers of gas chambers interleaved with 8 iron slabs and has a total thickness of approximately 1 m. The material in front of the HCAL amounts to 2.2 interaction lengths while the HCAL itself constitutes nearly 4 interaction lengths. Therefore, most hadronic showers will be initiated in or before the ECAL but will not reach beyond the HCAL. Studies estimate the energy resolution of the HCAL to be $\sigma_E/E = (100 - 140)\%/\sqrt{E}$. It is expected that nearly all muons above a certain energy will pass through the HCAL and reach the muon chambers.

The muon chambers lie outside of the HCAL and are designed for muon identification. The barrel section consists of four detector layers covering an angular region of $|\cos\theta| < 0.68$ with a fifth layer covering an angle of $|\cos\theta| < 0.72$. The layers are composed of a total of 110 drift chambers; each chamber has a width of 1.2 m and a depth of 90 mm. The layers are arranged in a staggered geometry to cause most muons to register in at least four layers. Muons are identified by matching tracks from the central tracking chambers with

signals generated in the muon chambers. The muon detector is able to measure particle positions in the ϕ direction with an accuracy of 1.5 mm and in the z direction with an accuracy of 2 mm.

Chapter 4

Event Selection

Data for this analysis has been collected from 1990 through 1994 with a total integrated luminosity of nearly 112 pb^{-1}. This represents approximately 160000 Z^0 decays to tau pairs. The branching ratios for the decays $\tau \to e\nu\nu$ and $\tau \to \mu\nu\nu$ have been measured to be $17.9 \pm 0.17\%$ and $17.44 \pm 0.23\%$ [36] respectively. Hence the fraction of tau pairs that both decay to leptons is approximately 3% for each of the four charged lepton decay pair cases: e^-e^+, $e^-\mu^+$, μ^-e^+, and $\mu^-\mu^+$. Thus there are expected to be a total of almost 20000 correlated leptonic tau decays in the data sample before selection. Although each of the four cases was examined, we will describe reasons for using only the $e^-\mu^+$ and μ^-e^+ cases in Chapter 5.

Various pieces of detector information must be combined in order to select out a relatively pure sample of correlated leptonic tau decays. The selection occurs in two phases. First, a set of criteria is applied to separate the Z^0 decays to tau pairs from the total sample. Each event selected is then examined to determine the decay type of each tau.

4.1 Tau Pair Selection

The standard OPAL tau pair selection is used for this analysis [44]. Before selection cuts may be applied a number of quantities must be specified. It is necessary to determine what minimum requirements must be passed to recognise a particle in the tracking chambers

and to define clusters in the electromagnetic calorimeter. A good charged track requires

$$N_{hit}(CJ) \geq 20 \tag{4.1}$$

$$P_t \geq 0.1\,\text{GeV} \tag{4.2}$$

$$|d_0| \leq 2\,\text{cm} \tag{4.3}$$

$$|z_0| \leq 75\,\text{cm} \tag{4.4}$$

$$|R_{min}| \leq 75\,\text{cm} \tag{4.5}$$

where $N_{hit}(CJ)$ is the number of hits in the jet chamber, P_t is the transverse momentum, $|d_0|$ is the distance of closest approach of the track to the beam axis, $|z_0|$ is the distance of the track from the interaction point along the beam axis and $|R_{min}|$ is the separation between the beam axis and the first hit in the jet chamber. In the electromagnetic calorimeter clusters are defined for later association to charged tracks or to particles invisible to the tracking chambers (eg. a photon). A cluster is a contiguous group of lead glass blocks containing a deposited energy of at least 20 MeV. A 'good' cluster is defined in the barrel region by

$$N_{blk} \geq 1 \tag{4.6}$$

$$E_{cls(raw)} \geq 0.1\,\text{GeV} \tag{4.7}$$

where N_{blk} is the number of lead glass blocks associated to the cluster and $E_{cls(raw)}$ is the total raw cluster energy assigned to the cluster.

The primary observable difference between multihadron production and lepton pair production from electron-positron annihilation is the number of charged particles created. For multihadron production the average charged particle multiplicity is greater than 20 over 90% of the time [45] while for lepton pair production the number of charged particles is less than 5 over 97% of the time. Hence, the multihadron background may be largely eliminated from the sample by requiring

$$1 \leq N_{chrg}^{Tot} \leq 6 \tag{4.8}$$

$$N_{clust}^{Tot} \leq 10 \tag{4.9}$$

where N_{chrg}^{Tot} is the total number of good charged particles measured in the event and N_{clust}^{Tot} is the number of well defined clusters.

The taus observed by OPAL have a large boost and hence the decay products are normally confined within a relatively narrow cone. Once lepton pairs have been selected from the sample it is useful to define jets for the association of particles to tau decays. A jet is defined by

$$\Theta_{half-cone} = 35^{\circ} \tag{4.10}$$

$$P_{cone} \geq 0.01 E_{beam} \tag{4.11}$$

$$N_{cone(chrg)} = 2 \tag{4.12}$$

where $\Theta_{half-cone}$ is the half angle of the cone around the direction constructed from the vector sum of track and ECAL cluster momenta associated to the cone, P_{cone} is the total energy in the cone and $N_{cone(chrg)}$ is the number of cones with at least one charged track.

Cosmic ray rejection cuts are based on the assumption that these background events will not appear to have originated at the interaction point and/or will exhibit timing measurements inconsistent with a true physics event. Such events are rejected by requiring that all physics events satisfy

$$|d_0|_{min} \leq 0.5 \text{ cm} \tag{4.13}$$

$$|z_0|_{min} \leq 20 \text{ cm} \tag{4.14}$$

$$|z_0|_{ave} \leq 20 \text{ cm} \tag{4.15}$$

where $|d_0|_{min}$ is the minimum $|d_0|$, $|z_0|_{min}$ is the minimum $|z_0|$ and $|z_0|_{ave}$ is the average $|z_0|$. In addition, an event is rejected unless at least one of the time-of-flight counters returns

$$|t_{mes} - t_{exp}| \leq 10 \text{ ns} \tag{4.16}$$

where t_{mes} is the measured time-of-flight and t_{exp} is the time-of-flight expected for an event generated at the nominal interaction point. An event is further rejected if all counter pairs satisfying

$$\delta\phi(i,j) \geq 165^{\circ} \tag{4.17}$$

measure

$$|t_i - t_j| \geq 10\,\text{ns} \tag{4.18}$$

where $\delta\phi(i,j)$ is the angular separation between counters i and j and $|t_i - t_j|$ is the measured time-of-flight difference.

A significant background may be introduced by two photon events. These events may mimic, for example, tau decays to correlated muon pairs or to correlated electron pairs. Such events are filtered by only accepting events with

$$\theta_{acol} \leq 15^\circ \tag{4.19}$$

$$E_{vis} = \sum_{cone} Max(E_{cls}, E_{trk}) \geq 0.03 E_{cm} \tag{4.20}$$

where θ_{acol} is the acolinearity between the two highest energy charged cones and E_{vis} is the total visible energy. For $P_t(cls)$ and $P_t(trk)$ equal to the transverse cluster momentum and track momentum respectively, events with $E_{vis} \leq 0.2 E_{beam}$ are removed if

$$P_t(cls) \leq 2\,\text{GeV} \tag{4.21}$$

$$P_t(trk) \leq 2\,\text{GeV}. \tag{4.22}$$

The majority of events passing the preceding cuts are expected to be lepton pair events. In other words $e^+e^- \rightarrow e^+e^-$, $e^+e^- \rightarrow \mu^+\mu^-$ or $e^+e^- \rightarrow \tau^+\tau^-$. Since it is assumed that no neutrinos are involved, electron pair events are characterised by total ECAL energy deposits near the centre of mass energy. Thus, these events may be screened out by requiring

$$\sum_i E_i(cls) \leq 0.8 E_{CM} \tag{4.23}$$

or

$$\sum_i E_i(cls) + 0.3 \sum_j E_j(trk) \leq E_{CM} \tag{4.24}$$

where the sum is over all cluster energies $E_i(cls)$ and all track energies $E_j(trk)$ in the event.

Lastly, an attempt must be made to remove the muon pair contamination from the remaining events. To proceed, events must first be recognised as containing two muons.

A particle is identified as a muon if it passes one of the following criteria:

$$N^{MU}_{layers} \geq 2 \tag{4.25}$$

or

$$N^{HC}_{layers} \geq 4, \quad N^{HC}_{last3} \geq 1 \quad and \quad N^{HC}_{hits/layer} > 2 \tag{4.26}$$

or

$$E_{cls} < 2\,\mathrm{GeV}. \tag{4.27}$$

Here, N^{MU}_{layers} is the number of layers registering a signal in the muon chambers, N^{HC}_{layers} is the number of HCAL layers associated with a track and registering a signal, $N^{HC}_{hits/layer}$ is the total number of HCAL hits divided by the total HCAL layers registering signal for the cone containing the track and E_{cls} is the relevant cluster energy. The third criterion 4.27 makes use of the minimum ionising property of muons. The first and second criteria reflect the fact that muons are expected to pass completely out of the detector. Once events have been tagged as dimuon events the muon pair events, which only contain particles that interact in the detector, are removed by requiring

$$\sum_{cone=1}^{2} [E^{clust}_{cone} + E^{track}_{cone}] \leq 0.6 E_{CM} \tag{4.28}$$

where E^{clust}_{cone} is the total cluster energy in each charged cone and E^{track}_{cone} is the track energy. It is anticipated that the events remaining in the sample are now largely tau pair events.

Once the tau pair selection has been completed, each charged cone identified with a tau must be examined to determine the possible decay type. This analysis is only concerned with events classified as purely leptonic tau decays.

4.2 Selection of Electronic Tau Decays

The selection of electron tau decays follows the standard OPAL algorithm [44] with the exception that the standard cut using angular information from PB is not employed here. A candidate cone is first inspected to determine the number of charged tracks it contains. The event is rejected unless

$$N_{chrg} \leq 2 \tag{4.29}$$

where N_{chrg} is the number of such tracks. Electrons in the tracking chambers sometimes radiate photons before reaching the ECAL. The radiated photons may then pair produce allowing more than one charged particle to appear in the cone. Hence, by allowing 2 charged tracks, such events are not summarily excluded. It is always assumed that the charged track exhibiting the largest momentum is the decay electron.

The ratio of cluster energy E_{cls} to track momentum p_{trk} is limited by the cut

$$0.7 < E_{cls}/p_{trk} < 2.0 \tag{4.30}$$

since it is expected that the measured momentum for electrons will be near the measured ECAL energy (figure 4.1). Hadronic tau decays typically give rise to showers in the ECAL that are not wholly contained. Conversely, tau decays to electrons normally produce comparatively confined showers allowing a straightforward matching between ECAL cluster and charged track. Hence, implementing the cut

$$E_{excess} < 0.04 E_{beam} \tag{4.31}$$

greatly reduces contamination by such hadronic decays. Here, E_{excess} is the total cluster energy assigned to the cone excluding the cluster associated to the electron candidate track. In particular, this cut suppresses tau decays that include $\pi^0 \rightarrow \gamma\gamma$. Figure 4.2 shows E_{excess}/E_{beam} both before and after selection.

An additional cut relying on the distinct shape of electron tau decays may be employed. The confined nature of the electron shower is emphasised by requiring

$$N_{blk}^{90} \leq 3 \tag{4.32}$$

where N_{blk}^{90} is the number of ECAL blocks containing at least 90 per cent of the cluster energy. Events displaying small measured ECAL energies are difficult to identify reliably and are removed with

$$x_e \equiv E_{cls}/E_{beam} > 0.05 \tag{4.33}$$

where E_{cls} is the total ECAL energy in the cone (figure 4.3).

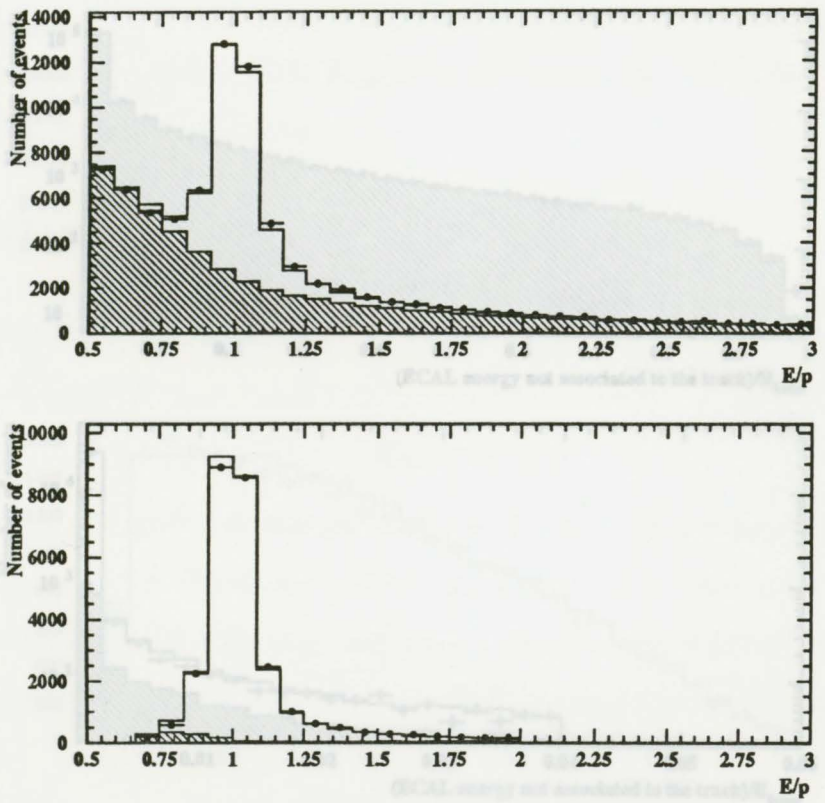

Figure 4.1: The top figure shows cluster energy over track momentum for all jets selected as taus. The bottom figure shows all jets selected as electron tau decays. Monte Carlo events are shown in the open histogram while the data is shown with error bars. The shaded section represents background Monte Carlo events.

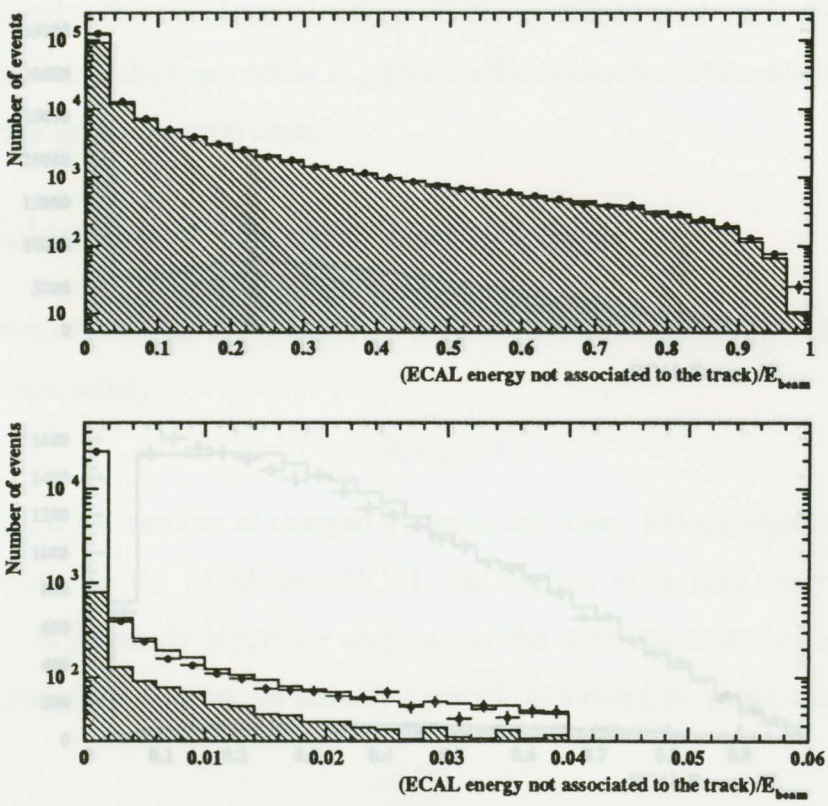

Figure 4.2: The top figure shows the excess cluster energy for all jets selected as taus. The bottom figure shows all jets selected as electron tau decays. Monte Carlo events are shown in the open histogram while the data is shown with error bars. The shaded section represents background Monte Carlo events.

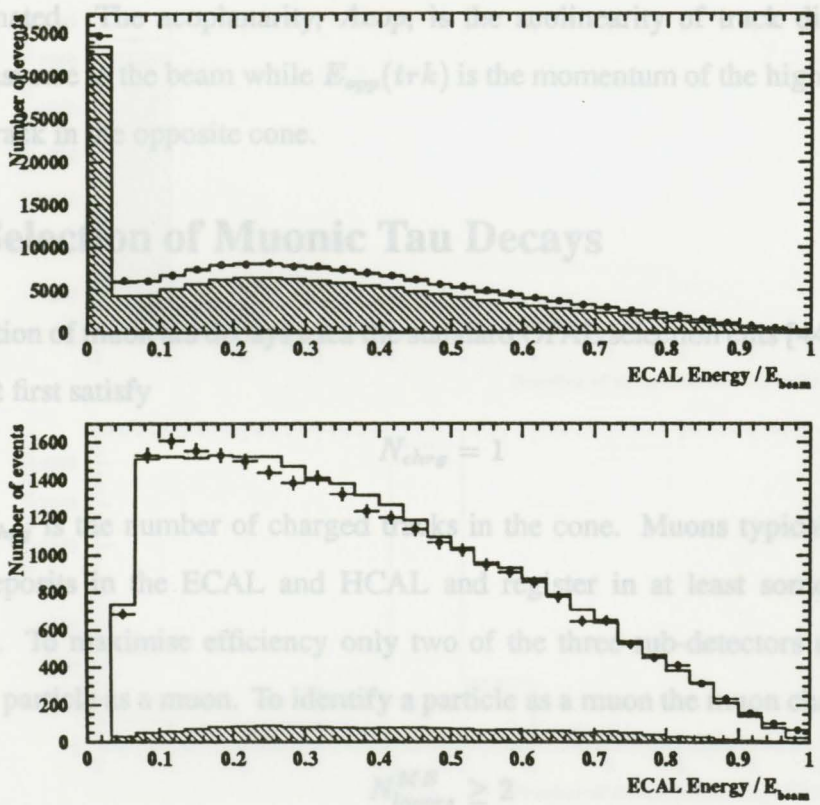

Figure 4.3: The top figure shows the electron variable x_e for all jets selected as taus. The bottom figure shows all jets selected as electron tau decays. Monte Carlo events are shown in the open histogram while the data is shown with error bars. The shaded section represents background Monte Carlo events.

Finally, it may happen that some electron pair events are included in the tau pair sample because one of the electron energies is measured incorrectly. To aid in reducing this background events in which the opposite track exhibits

$$E_{opp}(trk) > 0.75 E_{beam} \tag{4.34}$$

$$Acop < 0.1^{\circ} \tag{4.35}$$

are eliminated. The acoplanarity, $Acop$, is the acolinearity of track directions in the plane transverse to the beam while $E_{opp}(trk)$ is the momentum of the highest momentum charged track in the opposite cone.

4.3 Selection of Muonic Tau Decays

The selection of muon tau decays uses the standard OPAL selection cuts [44]. A candidate cone must first satisfy

$$N_{chrg} = 1 \tag{4.36}$$

where N_{chrg} is the number of charged tracks in the cone. Muons typically leave small energy deposits in the ECAL and HCAL and register in at least some of the muon chambers. To maximise efficiency only two of the three sub-detectors are required to identify a particle as a muon. To identify a particle as a muon the muon chambers require

$$N^{MB}_{layers} \geq 2 \tag{4.37}$$

where N^{MB}_{layers} is the number of layers registering signal associated to a charged track in the central tracking chambers (figure 4.4). In the hadron calorimeter, a particle is tagged as a muon if

$$N^{HC}_{layers} \geq 4 \tag{4.38}$$

$$N^{HC}_{hits/layer} < 3 \tag{4.39}$$

where N^{HC}_{layers} is the number of HCAL layers with signal corresponding to a candidate track and $N^{HC}_{hits/layer}$ is the total number of HCAL hits associated to the cone divided by

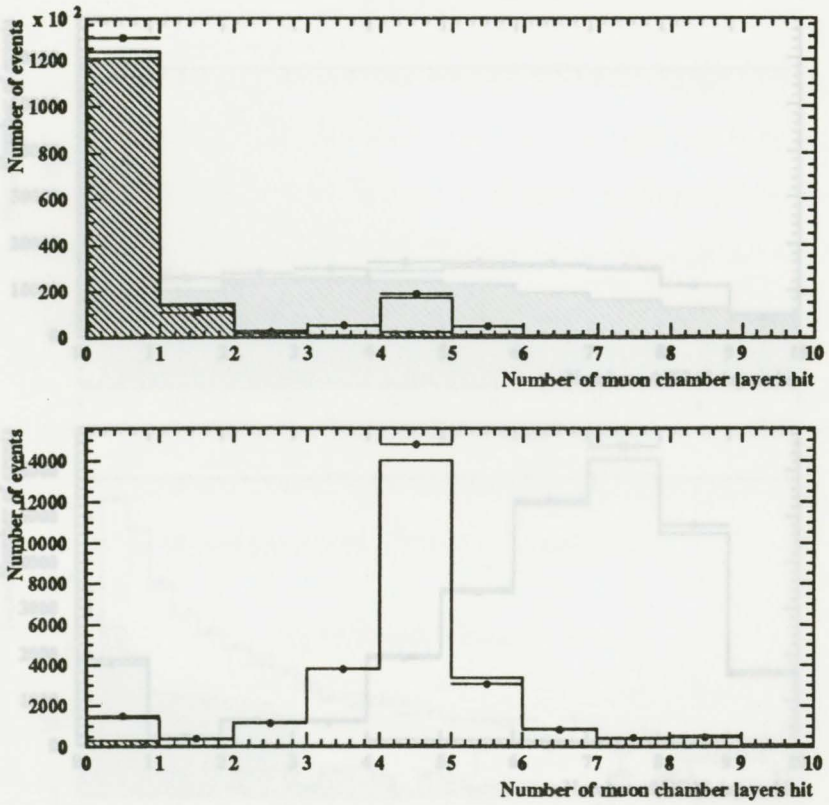

Figure 4.4: The top figure shows the number of muon layers containing a signal for all jets selected as taus. The bottom figure shows all jets selected as muon tau decays. Monte Carlo events are shown in the open histogram while the data is shown with error bars. The shaded section represents background Monte Carlo events.

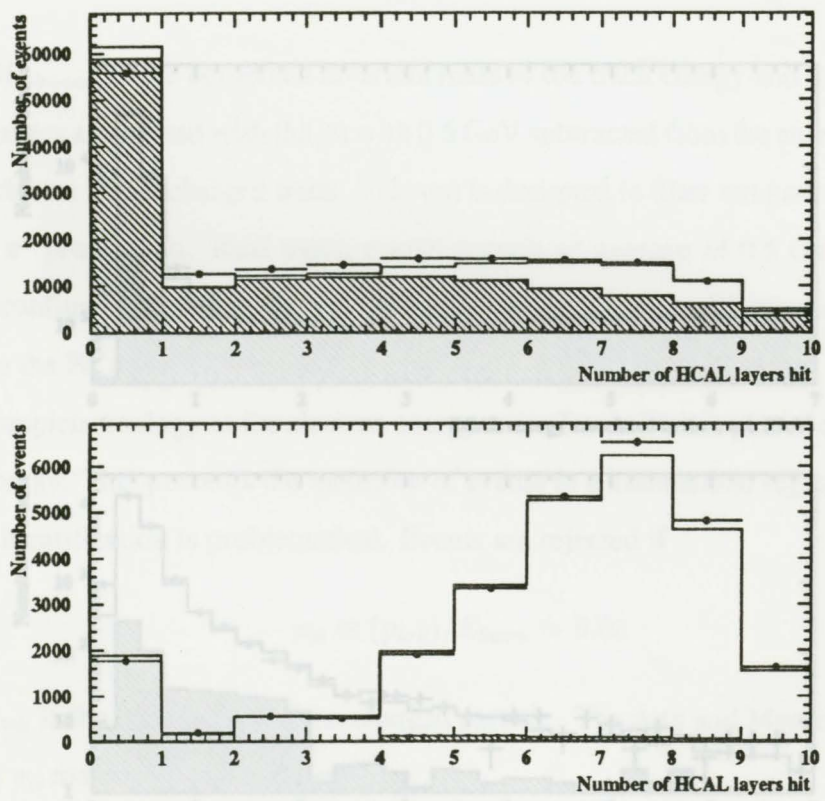

Figure 4.5: The top figure shows the number of HCAL layers containing a signal for all jets selected as taus. The bottom figure shows all jets selected as muon tau decays. Monte Carlo events are shown in the open histogram while the data is shown with error bars. The shaded section represents background Monte Carlo events.

N^{HC}_{layers} (figure 4.5). The ECAL is expected to measure only small energy losses from the passage of a muon and so a muon is identified by

$$E_{cls} < 2\,\text{GeV} \tag{4.40}$$

where E_{cls} is the cluster energy matched to the charged track. Figure 4.6 indicates the

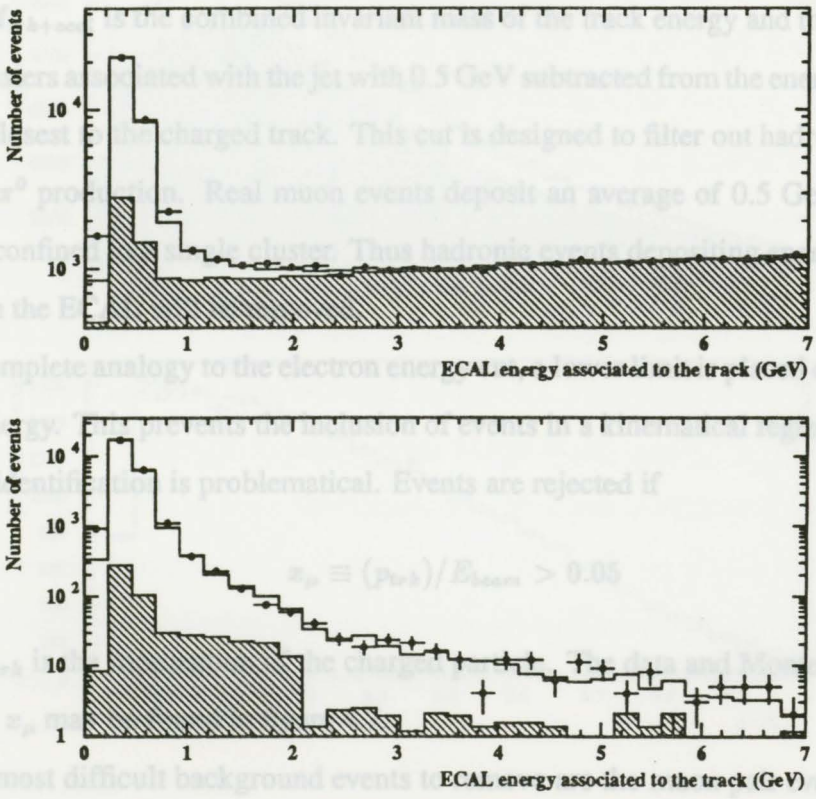

Figure 4.6: The top figure shows the cluster energy distributions for all jets selected as taus. The bottom figure shows all jets selected as muon tau decays. Monte Carlo events are shown in the open histogram while the data is shown with error bars. The shaded section represents background Monte Carlo events.

E_{cls} distributions before and after selection.

Muons are not expected to create large signals in the HCAL. Hence events are rejected

to reduce hadronic background if

$$N^{HC}_{layers} \geq 3 \tag{4.41}$$

$$N^{HC}_{hits/layer} \geq 3. \tag{4.42}$$

Further hadronic background is removed by the cut

$$M_{trk+ecal} < 0.3\,\text{GeV} \tag{4.43}$$

where $M_{trk+ecal}$ is the combined invariant mass of the track energy and the ECAL energy of all clusters associated with the jet with 0.5 GeV subtracted from the energy of the ECAL cluster closest to the charged track. This cut is designed to filter out hadronic decays that include π^0 production. Real muon events deposit an average of 0.5 GeV in the ECAL usually confined to a single cluster. Thus hadronic events depositing energy over a larger region in the ECAL will be removed.

In complete analogy to the electron energy cut, a lower limit is placed on the measured muon energy. This prevents the inclusion of events in a kinematical region where correct particle identification is problematical. Events are rejected if

$$x_\mu \equiv (p_{trk})/E_{beam} > 0.05 \tag{4.44}$$

where p_{trk} is the momentum of the charged particle. The data and Monte Carlo distributions for x_μ may be found in figure 4.7.

The most difficult background events to remove are the muon pair events. To reduce this background, a check is made on the opposite cone to determine whether it appears to be a high energy muon. The opposite jet is assumed to contain a muon if it passes the muon chamber identification above or it passes the HCAL identification or it passes through a region where the HCAL and muon chambers are not fully active. If the opposite cone is tagged with a muon then the event is rejected if

$$x_{\mu(opp)} \geq 0.8 \tag{4.45}$$

where $x_{\mu(opp)}$ is the scaled energy of the proposed muon in the opposite cone.

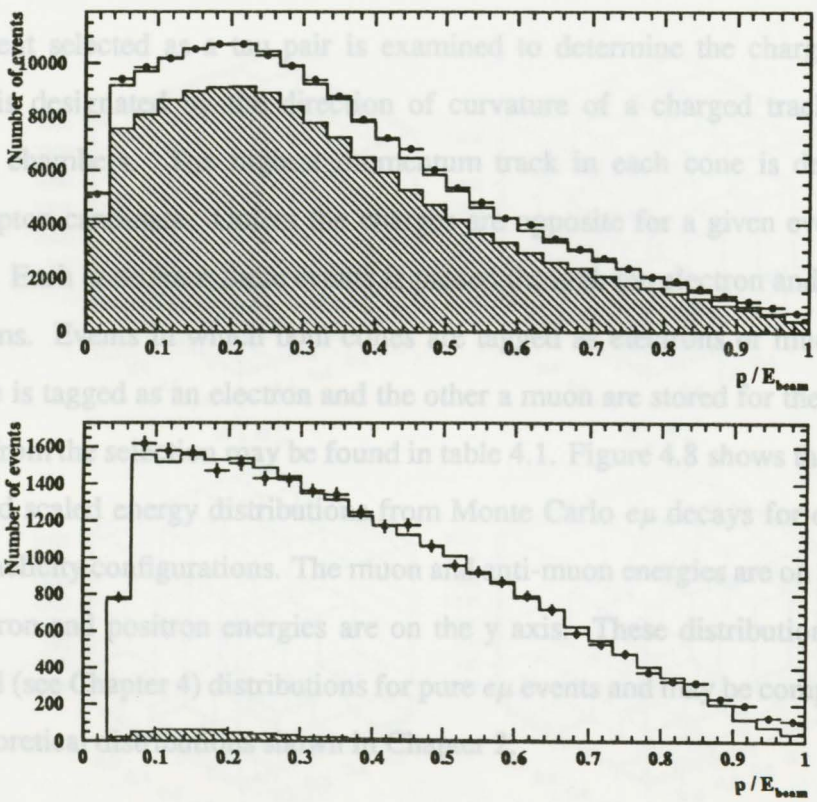

Figure 4.7: The top figure shows the muon energy variable x_μ distribution for all jets selected as taus. The bottom figure shows all jets selected as muon tau decays. Monte Carlo events are shown in the open histogram while the data is shown with error bars. The shaded section represents background Monte Carlo events.

	e^-e^+	$\mu^-\mu^+$	$e^-\mu^+$	μ^-e^+
Events Selected	2003	1769	2044	2100

Table 4.1: Physics events selected as leptonic tau decay pairs.

4.4 Simultaneous Leptonic Decays

Each event selected as a tau pair is examined to determine the charge configuration. Charge is designated by the direction of curvature of a charged track in the central tracking chambers. The highest momentum track in each cone is designated as the decay lepton candidate. Unless the charges are opposite for a given event, the event is rejected. Each cone from these events is passed through the electron and muon selection algorithms. Events in which both cones are tagged as electrons or muons or in which one cone is tagged as an electron and the other a muon are stored for the fit to ξ and P_τ. Results from the selection may be found in table 4.1. Figure 4.8 shows the reconstructed, correlated scaled energy distributions from Monte Carlo $e\mu$ decays for each of the four tau pair helicity configurations. The muon and anti-muon energies are on the x axis while the electron and positron energies are on the y axis. These distributions represent the corrected (see Chapter 4) distributions for pure $e\mu$ events and may be compared to the tree level theoretical distributions shown in Chapter 2.

4.5 Monte Carlo

To control background contamination and estimate efficiency, several Monte Carlo sets are employed. The tau pair and muon pair Monte Carlo sets were generated using the KORALZ program [46]. The electron pair events were generated using the BABAMC [47] program and the two photon Monte Carlo events were generated using the Vermaseren program [48]. To estimate non-tau background contributions, electron pair, muon pair and two photon (ee and $\mu\mu$) events were examined. Standard Model tau decay Monte Carlo events were employed to determine the tau pair selection efficiency and to estimate tau

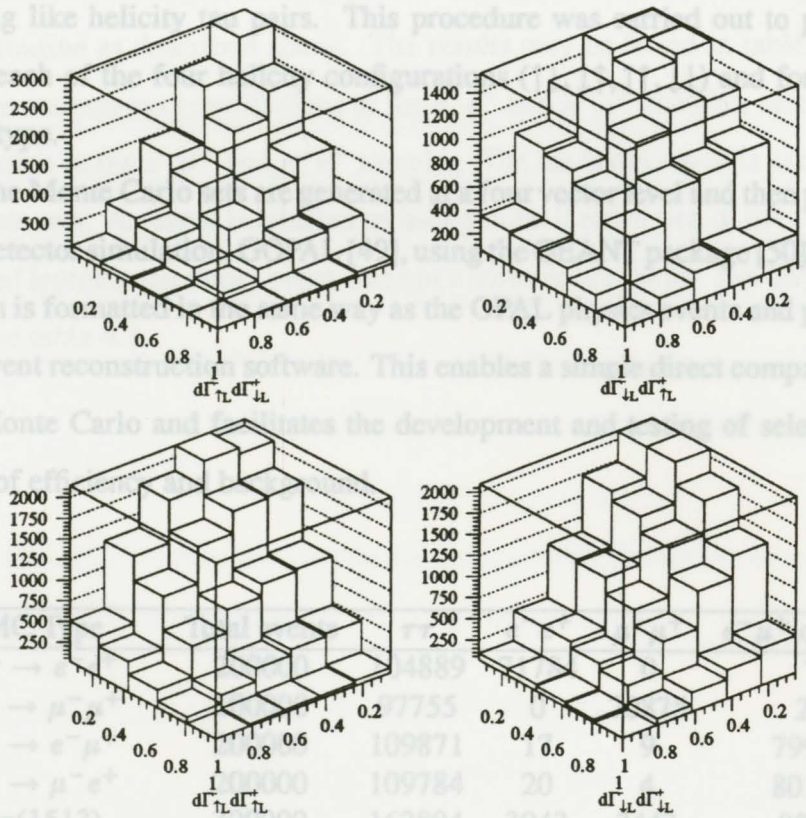

Figure 4.8: Reconstructed correlated energy distributions for pure $e\mu$ events after selection. The histograms have been filled from the $e\mu$ Monte Carlo events created for this analysis.

background sources. The tau pair events consisted of two separately created Monte Carlo runs which we will denote '1513' and '1520'.

Finally, for each of the simultaneous leptonic decay pair types, four sets of different tau helicity configuration events were generated. KORALZ creates events with definite tau helicity and uses the V-A Standard Model interaction to generate leptonic decay particles. By default, tau pair events are generated with opposite helicities. However, as discussed in Chapter 2, events simulating V+A interactions may be generated using the V-A coupling and creating like helicity tau pairs. This procedure was carried out to produce 50000 events for each of the four helicity configurations ($\uparrow\downarrow, \downarrow\uparrow, \uparrow\uparrow, \downarrow\downarrow$) and for each leptonic decay pair type.

All of the Monte Carlo sets are generated at a four vector level and then passed through an OPAL detector simulation, GOPAL [49], using the GEANT package [50]. The resulting information is formatted in the same way as the OPAL physics events and passed through the same event reconstruction software. This enables a simple direct comparison between data and Monte Carlo and facilitates the development and testing of selection cuts and estimation of efficiency and background.

MC Type	Total events	$\tau\tau$	e^-e^+	$\mu^-\mu^+$	$e^-\mu^+$ or μ^-e^+
$\tau\tau \rightarrow e^-e^+$	200000	104889	71784	0	7
$\tau\tau \rightarrow \mu^-\mu^+$	200000	97755	0	70875	29
$\tau\tau \rightarrow e^-\mu^+$	200000	109871	17	9	79998
$\tau\tau \rightarrow \mu^-e^+$	200000	109784	20	4	80138
$\tau\tau(1513)$	300000	162804	3943	3443	8256
$\tau\tau(1520)$	538275	292948	6877	6006	14892
$e^-e^+ \rightarrow e^-e^+$	714966	344	11	0	0
$e^-e^+ \rightarrow \mu^-\mu^+$	599331	1582	0	8	9
$e^-e^+ \rightarrow \gamma\gamma(ee)$	186042	133	50	0	0
$e^-e^+ \rightarrow \gamma\gamma(\mu\mu)$	246633	141	0	84	0

Table 4.2: Results of selection routines on Monte Carlo data. The top four samples are the leptonic tau decay pair events generated specifically for this analysis. The middle two sets are the general tau decay events generated at CERN. The last four samples are used to estimate non-tau background.

Event Type	Background(1513)	Background(1520)
ee	479	778
$\mu\mu$	189	251
$e\mu(combined)$	743	1130

Table 4.3: Background from non-leptonic tau decays.

The Monte Carlo sets were each passed through the simultaneous leptonic tau decay selection routine as described above. The results may be found in table 4.2. Note that, while there are non-tau contributions to the e^-e^+ and $\mu^-\mu^+$ samples, there is virtually no contamination in the $e^-\mu^+$ and μ^-e^+ samples. The tau background is estimated from the tau pair data sets. An event is labelled as background if either one of the cones selected as a correlated leptonic tau decay event was not a leptonic tau decay. Tau background results are listed in table 4.3.

Chapter 5

Analysis

Although we have constructed a theoretical distribution in equation 2.17 it is not representative of the distribution we actually measure and must be corrected for a number of effects. The dominant contributing correction factors may be separated into four types: radiative, resolution, efficiency and background. The various correction factors may depend upon charge, helicity, energy and other measured quantities.

5.1 Corrections

Using equation 2.25 we may incorporate the various correction factors in a straight forward manner. To simplify the notation we will define the quantities

$$\begin{aligned} N^{ud} &\equiv d\Gamma^{-}_{\uparrow L}(x_1)d\Gamma^{+}_{\downarrow L}(x_2) \\ N^{du} &\equiv d\Gamma^{-}_{\downarrow L}(x_1)d\Gamma^{+}_{\uparrow L}(x_2) \\ N^{uu} &\equiv d\Gamma^{-}_{\uparrow L}(x_1)d\Gamma^{+}_{\uparrow L}(x_2) \\ N^{dd} &\equiv d\Gamma^{-}_{\downarrow L}(x_1)d\Gamma^{+}_{\downarrow L}(x_2). \end{aligned} \tag{5.1}$$

At the tree level, the fit function is then

$$\begin{aligned} N^{fit} = K[&\frac{1}{4}(1+\xi^2+\xi P_\tau)N^{ud} \\ &+\frac{1}{4}(1+\xi^2-\xi P_\tau)N^{du} \\ &+\frac{1}{2}(1-\xi^2)(N^{uu}+N^{dd})] \end{aligned} \tag{5.2}$$

where the overall normalisation is K events. Notice that we have changed the coefficient of the $N^{uu} + N^{dd}$ term from $\frac{1}{4}$ to $\frac{1}{2}$. In equation 2.25 each of the four two dimensional distributions are normalised to unity. When we apply this form to the fitting routine the sum $N^{uu} + N^{dd}$ will be normalised to unity.

Corrections may now be applied to each of the four distributions separately. Symbolically we may write each of the corrected distributions as

$$N_{corr} = N_{tree} R r \epsilon + \beta \tag{5.3}$$

where R is the detector resolution correction factor, r is the radiative correction factor, ϵ is the decay mode selection efficiency and β is the tau background. R, ϵ and β do not depend directly on the functional forms of 5.1. As discussed in Chapter 2, radiative corrections do alter the theoretical functional forms but in such a way as to preserve 2.23. Hence the assumptions employed to construct 2.25 remain valid. In addition to the decay mode selection efficiency and the tau background we must correct for the tau selection efficiency ϵ_τ and the non-tau background $\beta_{non-\tau}$. The fully corrected theoretical distribution is then

$$\begin{aligned} N_{corr}^{fit} = K[\{&\frac{1}{4}(1+\xi^2+\xi P_\tau)(N_{tree}^{ud} R^{ud} r^{ud} \epsilon^{ud} + \beta^{ud}) \\ &+\frac{1}{4}(1+\xi^2-\xi P_\tau)(N_{tree}^{du} R^{du} r^{du} \epsilon^{du} + \beta^{du}) \\ &+\frac{1}{2}(1-\xi^2)((N_{tree}^{uu} R^{uu} r^{uu} \epsilon^{uu} + \beta^{uu}) + (N_{tree}^{dd} R^{dd} r^{dd} \epsilon^{dd} + \beta^{dd}))\}\epsilon_\tau \\ &+\beta_{non-tau}]. \end{aligned} \tag{5.4}$$

The practical implementation of the correction factors may proceed in a number of ways. We have chosen to create Monte Carlo distributions that incorporate the corrections directly. As discussed in Chapter 4, the generated Monte Carlo sets include radiative corrections to order α and are passed through a detector simulation. The tau background is introduced using the tau pair Monte Carlo events. The correlated lepton pair distributions were generated specifically for this analysis and correspond to each of the $N_{tree} R r \epsilon$ terms in 5.4. Non-tau background sources are expected to be small and were examined using the two photon, electron pair and muon pair Monte Carlo samples and will be discussed below. The contribution of hadronic non-tau background is expected to be small [44].

The tau pair Monte Carlo sets only include events in which the tau helicities are opposite. As discussed in Chapter 4, the N^{uu} and N^{dd} distributions were generated from like helicity tau pair events. Hence, we may not estimate the tau background for the like helicity events directly. Instead, single particle distributions are multiplied to simulate this background.

For illustrative purposes, example distributions for each of the correction factors are presented. This gives an indication of the relative effect of each correction type.

5.1.1 Radiative Corrections

As discussed in the theory section, equation 2.17 is only a tree level approximation and hence higher order radiative corrections must be accounted for. Since the Monte Carlo generator KORALZ includes radiative corrections to $O(\alpha)$ it is easiest to calculate these corrections with Monte Carlo samples. The four vector values from a sample of 100000 $\tau\tau \rightarrow e\mu$ events were used to create the expected Standard Model distribution. The events were binned in 25 equally sized bins with respect to the x_e and x_μ variables and then divided by equation 2.17. The five slices in x_e of the resulting fractional radiative correction histogram as a function of x_μ may be found in figure 5.1.

5.1.2 Resolution

The second effect we must correct for is that of the detector apparatus on the measured particles. We have an imperfect knowledge of materials and particle interactions with them but from test beam experiments and previous analyses we may deduce the general effects of the detector pieces on measured particle energies. OPAL's GOPAL [49] software has been designed to simulate such effects. Monte Carlo events were binned after decay mode selection first using the four vector generated x_e and x_μ values and then using the reconstructed values. Figure 5.2 shows the ratio of the reconstructed distribution and the four vector distribution assuming a Standard Model interaction.

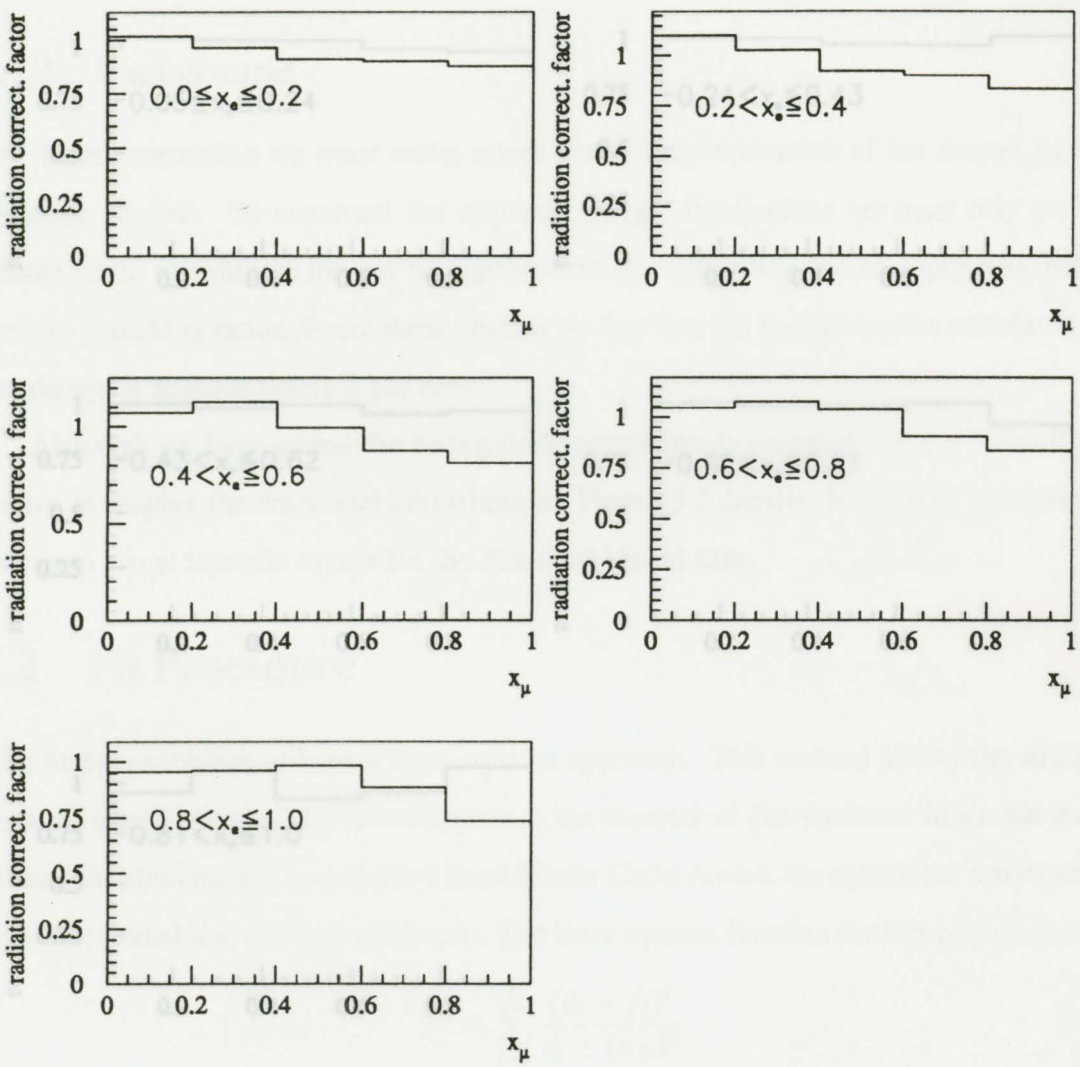

Figure 5.1: Shown are the fractional radiative corrections. The five histograms represent slices in x_e of the correlated $e\mu$ distribution as functions of x_μ.

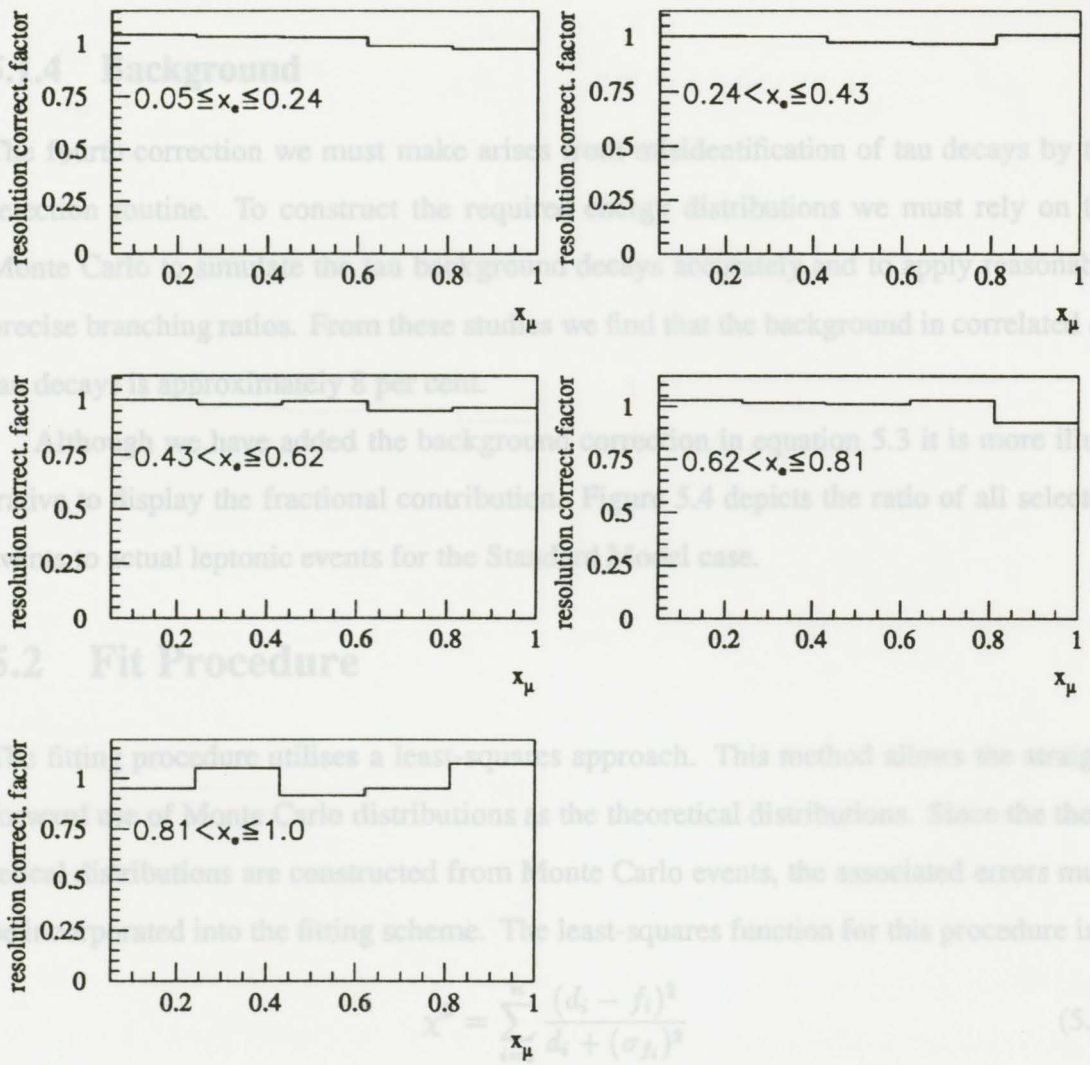

Figure 5.2: Shown are the fractional resolution corrections. The five histograms represent slices in x_e of the correlated $e\mu$ distribution as functions of x_μ.

5.1.3 Efficiency

The third correction arises from the efficiency of the selection routine. Efficiency is defined here as the four vector x distribution after tau decay selection divided by the four vector x distribution before selection. The ratio of these quantities is shown in figure 5.3 for a Standard Model interaction.

5.1.4 Background

The fourth correction we must make arises from misidentification of tau decays by the selection routine. To construct the required energy distributions we must rely on the Monte Carlo to simulate the tau background decays accurately and to apply reasonably precise branching ratios. From these studies we find that the background in correlated $e\mu$ tau decays is approximately 8 per cent.

Although we have added the background correction in equation 5.3 it is more illustrative to display the fractional contribution. Figure 5.4 depicts the ratio of all selected events to actual leptonic events for the Standard Model case.

5.2 Fit Procedure

The fitting procedure utilises a least-squares approach. This method allows the straight forward use of Monte Carlo distributions as the theoretical distributions. Since the theoretical distributions are constructed from Monte Carlo events, the associated errors must be incorporated into the fitting scheme. The least-squares function for this procedure is

$$\chi^2 = \sum_{i=1}^{n} \frac{(d_i - f_i)^2}{d_i + (\sigma_{f_i})^2} \tag{5.5}$$

where d_i is the number of data events in bin i of the n bins, f_i is the number of total predicted events in bin i and σ_{f_i} is the error contributed by the Monte Carlo distributions. The f_i depend on the Monte Carlo sources through

$$f_i = N_D \sum_{j=1}^{m} P_j a_{ji} / N_j. \tag{5.6}$$

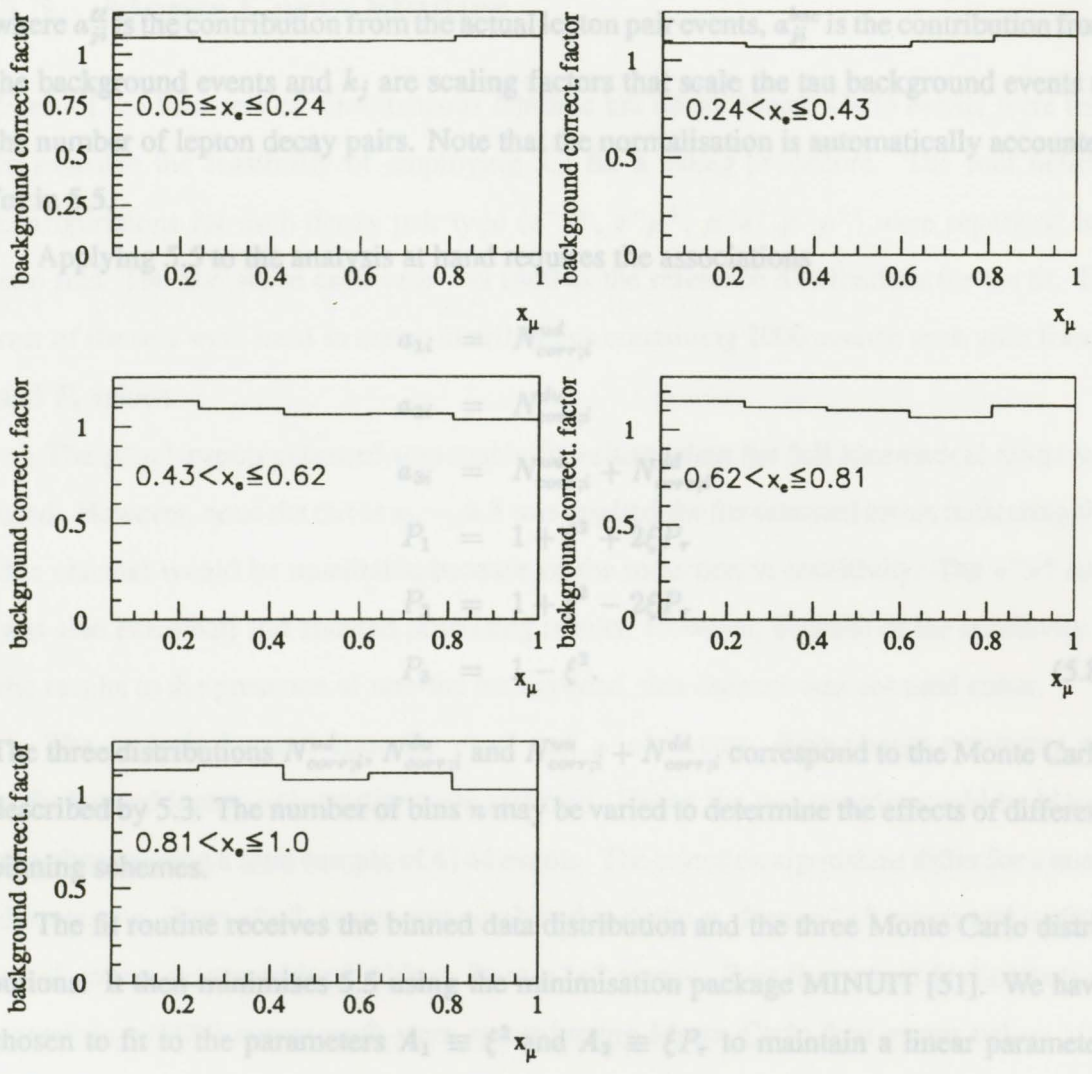

Figure 5.4: Shown are the fractional background corrections. The five histograms represent slices in x_e of the correlated $e\mu$ distribution as functions of x_μ.

Here, N_D is the total number of data events, N_j is the total number of Monte Carlo events in source j, P_j is the relative strength of source j and a_{ji} is the number of events in bin i of the j^{th} source. The Monte Carlo error is calculated using

$$\sigma_{f_i}^2 = N_D^2 \sum_j P_j^2 [a_{ji}^{ll} + k_j^2 a_{ji}^{bac}]/N_j^2 \tag{5.7}$$

where a_{ji}^{ll} is the contribution from the actual lepton pair events, a_{ji}^{bac} is the contribution from the background events and k_j are scaling factors that scale the tau background events to the number of lepton decay pairs. Note that the normalisation is automatically accounted for in 5.5.

Applying 5.5 to the analysis at hand requires the associations

$$\begin{aligned} a_{1i} &= N_{corr;i}^{ud} \\ a_{2i} &= N_{corr;i}^{du} \\ a_{3i} &= N_{corr;i}^{uu} + N_{corr;i}^{dd} \\ P_1 &= 1 + \xi^2 + 2\xi P_\tau \\ P_2 &= 1 + \xi^2 - 2\xi P_\tau \\ P_3 &= 1 - \xi^2. \end{aligned} \tag{5.8}$$

The three distributions $N_{corr;i}^{ud}$, $N_{corr;i}^{du}$ and $N_{corr;i}^{uu} + N_{corr;i}^{dd}$ correspond to the Monte Carlo described by 5.3. The number of bins n may be varied to determine the effects of different binning schemes.

The fit routine receives the binned data distribution and the three Monte Carlo distributions. It then minimises 5.5 using the minimisation package MINUIT [51]. We have chosen to fit to the parameters $A_1 \equiv \xi^2$ and $A_2 \equiv \xi P_\tau$ to maintain a linear parameter dependence as nearly as possible. MINUIT returns the fit parameters A_1 and A_2 along with error estimates. These errors are calculated in two different ways. The first method assumes that a parabolic approximation is valid for the shape of the χ^2 function near the minimum. MINUIT calculates the second derivative matrix and inverts it to determine the errors. For the second method, error estimates are calculated by determining the variation in each parameter when the χ^2 function is increased by 1.0. The errors from

the second method are expected to almost always be correct. The difference between the two errors gives an indication of the non-linearity of the fitting function with respect to the parametrisation chosen. These errors will correspond to one standard deviation limits. The fit parameters and their errors may then be converted to estimates on ξ and P_τ.

5.3 Monte Carlo Studies

Each of the four sets of simultaneous leptonic tau decay Monte Carlo events were used to examine the feasibility of employing 5.2 for a fitting procedure. The four helicity configurations for each decay pair type (e^-e^+, $e^-\mu^+$, μ^-e^+,$\mu^-\mu^+$) were separated into two sets. The first set in each case was used as the reference distributions for the fit. The rest of the sets were used to create distributions containing 2000 events; each with fixed ξ and P_t values.

The $\mu^-\mu^+$ events returned reasonable fit values when the full kinematical range was used. However, once the cut at $x_\mu = 0.8$ was applied the fits returned errors indicating that this channel would be unsuitable because of the reduction in sensitivity. The e^-e^+ case was also examined and showed promising results. However, because of the sensitivity of the results to the presence of non-tau background, this channel was not used either.

The analysis focused upon the $e^-\mu^+$ and μ^-e^+ events. Both charge symmetry and right handed lepton universality were assumed. Hence the two samples could be binned together creating a total sample of 4144 events. The selection algorithms differ for e and μ decays so x_μ from $e^-\mu^+$ events was combined with the x_μ from μ^-e^+ events and x_e from $e^-\mu^+$ events was combined with x_e from μ^-e^+ events. Four theoretical fit distributions containing 18000 events each were created using Monte Carlo four vector values after tau selection. The remaining events were used to construct fifteen sets of 4000 event histograms. These histograms were then used as test 'data'. Each of the 15 samples was fitted using the procedure outlined above for each of three bin sizes: 4 by 4, 5 by 5 and 6 by 6. These studies test both the Monte Carlo sets and the fitting procedure itself. In each case the standard deviation of the fit parameters agreed well with the mean errors returned by MINUIT and the central values were constistent with the input parameters.

An analogous set of fits was then carried out using events tagged by the decay mode selection algorithms and employing the reconstructed energy values. Each theoretical fit distribution was filled with 18000 events while 8 test 'data' samples of 4000 events each were created. The fit values were again consistent with the input values within statistical fluctuations and the errors from the fit were consistent with the spread of the 8 fitted values. From this study we conclude that the fit is unbiased and the errors from the fit procedure are consistent with expectations. We note that before background contributions are added a statistical error on the order of 0.35 for A_1 and 0.06 for A_2 may be expected for 4000 data events.

5.4 Data Fit and Systematic Checks

The Monte Carlo studies indicated that no particular bin scheme was preferred. To minimise the number of bins containing small counts while maximising sensitivity a 5 by 5 binning was employed. A binned χ^2 fit was carried out using the fully corrected Monte Carlo distributions on the 4144 selected data events. Minimisation of the χ^2 function produced the results

$$A_1 = 0.63 \pm 0.51$$

$$A_2 = -0.218 \pm 0.062.$$

The χ^2 function at the minimum was 30.76 for 23 degrees of freedom. The probability that the χ^2 is greater than 30.76 is 13%. Figure 5.5 shows the fit result plotted over the data in 5 slices of x_e as a function of x_μ. The generated errors are consistent with those anticipated from the Monte Carlo study. They represent the statistical error of the data set and of the finite size of the Monte Carlo theoretical distributions. It is necessary to examine possible systematic effects arising from the selection and fit procedures.

Energy scale and resolution systematic effects were studied in two ways. First, the electron and muon energies for the data were scaled absolutely by $\pm 0.5\%$. Secondly, a Gaussian smearing was applied to the Monte Carlo by adding a randomly generated value to each electron and muon reduced energy. For the electron energy, an examination of

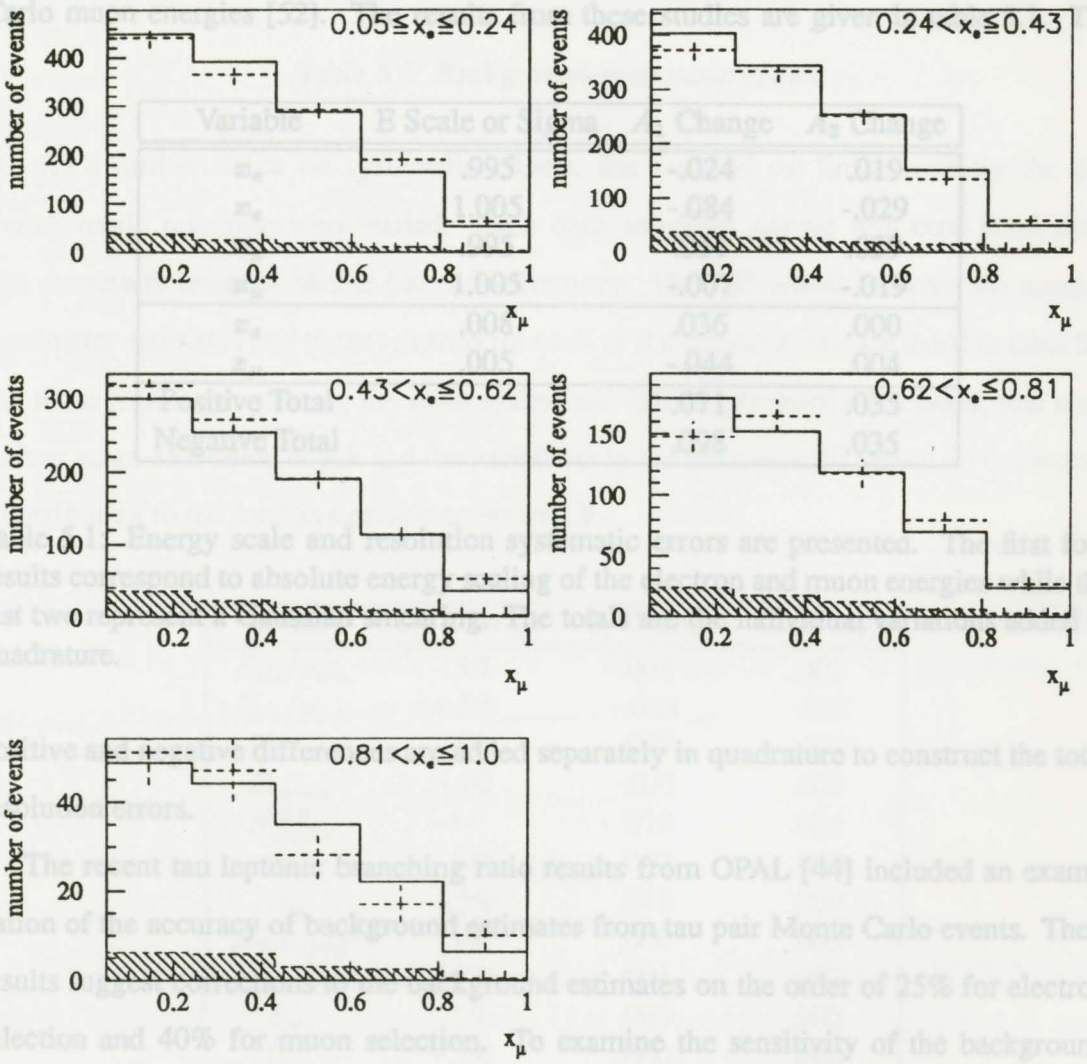

Figure 5.5: Shown is the correlated data histogram versus the Monte Carlo distribution corresponding to the parameter fit estimates for 5 slices of x_e as a function of x_μ. The dashed lines with error bars represent the data while the open histograms represent the Monte Carlo. The hatched histogram indicates the Monte Carlo estimated background contribution.

the E_{cls}/p_{trk} variable (see figure 4.1) indicated that a smearing with $\sigma = 0.008$ would approximate the discrepancy between the data and Monte Carlo E_{cls}/p_{trk} distributions. For the muon Monte Carlo energies, previous work showed that a standard deviation of $\sigma = 0.005$ would approximately account for differences between the data and Monte Carlo muon energies [52]. The results from these studies are given in table 5.1. The

Variable	E Scale or Sigma	A_1 Change	A_2 Change
x_e	.995	-.024	.019
x_e	1.005	-.084	-.029
x_μ	.995	.061	.029
x_μ	1.005	-.007	-.019
x_e	.008	.036	.000
x_μ	.005	-.044	.004
Positive Total		.071	.035
Negative Total		.098	.035

Table 5.1: Energy scale and resolution systematic errors are presented. The first four results correspond to absolute energy scaling of the electron and muon energies while the last two represent a Gaussian smearing. The totals are the individual variations added in quadrature.

positive and negative differences are added separately in quadrature to construct the total resolution errors.

The recent tau leptonic branching ratio results from OPAL [44] included an examination of the accuracy of background estimates from tau pair Monte Carlo events. Their results suggest corrections to the background estimates on the order of 25% for electron selection and 40% for muon selection. To examine the sensitivity of the background estimates on the fit results in this analysis, we scaled the background contribution to the theoretical distributions by 0.5 and 1.5 which more than accounts for the 25% and 40% uncertainties. Table 5.2 presents the results from this study.

The full fit result including both statistical and combined systematic errors is then

$$\begin{aligned} A_1 &= 0.63 \pm 0.51^{+0.07}_{-0.17} \\ A_2 &= -0.218 \pm 0.062 \pm 0.035 \end{aligned} \tag{5.9}$$

Bkg. Scale	A_1 Change	A_2 Change
.5	.009	.000
1.5	-.144	.003
Pos. Total	.009	.003
Neg. Total	.144	.000

Table 5.2: Background systematic errors.

As a further check on systematic effects, the nominal cut limits used for the data decay mode selection were varied. Each data selection sample was then fitted using the nominally selected Monte Carlo distributions. The differences between the nominal parameter estimates and those returned for each of the cut variations are listed in table 5.3. As these results are probing the same systematic effects previously discussed, this study serves as an additional check and the variations in the parameter fit values do not make a contribution to the total systematic errors in 5.9

Variable	Cut Change	A_1 Change	A_2 Change
E_{cls}/p_{trk}	-.5%	.001	.002
E_{cls}/p_{trk}	+.5%	-.023	-.002
E_{excess}	-.03	.029	-.019
E_{excess}	+.02	-.077	.009
N^{HB}_{layers}	+1	.019	.065
x_e	-.5%	.007	.000
x_e	+.5%	.016	.000
$M_{trk-ecal}$	-1%	.000	.000
$M_{trk-ecal}$	+1%	.003	.002
E_{cls}	-.5%	.000	.000
E_{cls}	+.5%	.000	.000
$N^{HC}_{hits/layer}$	+1	.008	.042
$x_\mu(lower)$	-.5%	.007	.000
$x_\mu(lower)$	+.5%	.016	.000
$x_\mu(upper)$	-.5%	.000	.000
$x_\mu(upper)$	+.5%	.000	.000

Table 5.3: Efficiency systematic cross checks.

Chapter 6

Results and Discussion

In Chapter 5 the results from this analysis were presented in the form of the two parameters A_1 and A_2 where

$$A_1 = \xi^2$$
$$A_2 = \xi P_\tau \tag{6.1}$$

These results have assumed that ξ was given by the relation 2.14 and that ξ is the same irrespective of the leptonic decay channel or the charge of the tau. Calculating the corresponding values of ξ and P_τ from equation 6.1 gives

$$|\xi| = 0.79^{+0.28+0.05}_{-0.44-0.11}$$
$$|P_\tau| = 0.276^{+0.35+0.057}_{-0.10-0.038} \tag{6.2}$$

In 6.2 we have only shown the magnitude of the parameters. In fact, we do have the relative sign information since we have measured ξP_τ to be negative. Thus ξ and P_τ must have opposite signs. We can utilise other experimental information to fix the absolute signs.

The tau polarisation is related to the neutral weak vector and axial couplings through

$$P_\tau = -\frac{2\hat{g}_V^\tau/\hat{g}_A^\tau}{1+(\hat{g}_V^\tau/\hat{g}_A^\tau)^2} \tag{6.3}$$

where $\hat{g}_V^\tau$ and $\hat{g}_A^\tau$ are the effective vector and axial-vector neutral weak coupling constants for tau particles.

At the SLAC linear collider, the use of polarised e^-e^+ beams allows the measurement of the left-right asymmetry

$$A_{LR} = (\sigma_L - \sigma_R)/(\sigma_L + \sigma_R) \tag{6.4}$$

where $\sigma_{L(R)}$ is the total Z production cross-section for a left-handed (right-handed) polarisation of the electron beam. This left-right asymmetry measures the neutral weak coupling constants for electrons. If we assume lepton universality in the neutral weak sector then the tau polarisation is related to A_{LR} by the relation $P_\tau = -A_{LR}$. The SLD group at SLAC has obtained the result [53]

$$A_{LR} = 0.1628 \pm 0.0071 \pm 0.0028 \tag{6.5}$$

which we will interpret as determining the sign of the tau polarisation to be negative. Thus we find that $\xi = +0.79^{+0.28+0.05}_{-0.44-0.11}$ and $P_\tau = -0.276^{+0.35+0.057}_{-0.10-0.038}$. The value of ξ is consistent with a pure V-A charged weak interaction while the P_τ value is consistent with the neutral current measurement given in 6.5.

6.1 Tau Decay Results

The accumulation of tau events over the last decade has enabled physicists to determine experimental values for several of the tau decay Michel parameters. The most easily accessible parameter is the ρ since it only affects the shape of the decay lepton energy distribution. In addition, a measurement of ρ does not require the decay of polarised tau particles.

A number of experiments [54] [55] [56] have analysed the electron and muon one dimensional energy distributions from tau decays to determine ρ. The current world average is $\rho = 0.74 \pm 0.04$ [36]. This value assumes that ρ is the same for both electron and muon tau decays and is consistent with a V-A interaction.

To date, only two measurements of the δ parameter in leptonic tau decays have been made. Equation 2.12 indicates that confining an analysis to the decay lepton energy distribution will enable one to measure the product $\xi\delta$. The ALEPH experiment has

determined the value $\xi\delta = 0.88 \pm 0.11 \pm 0.07$ [34] while the ARGUS Collaboration has found $\xi\delta = 0.77^{+0.18}_{-0.16} \pm 0.05$ [33]. If one assumes $\xi = 1$ then these results are consistent with a V-A interaction.

The focus of this analysis has been to extract a measurement of ξ while assuming ρ and δ to be exactly equal to their Standard Model values. Currently, there exist three measurements of the ξ parameter for leptonic tau decays. In 1993, the ARGUS group [32] used a procedure similar to ours to measure $|\xi| = 0.90 \pm 0.15 \pm 0.10$.

Both ARGUS and ALEPH have published measurements of ξ within the last year. ARGUS has found $\xi = 1.26^{+0.30}_{-0.26} \pm 0.09$. In this result they are able to determine the sign of ξ by using hadronic tau decays in their fit. The ALEPH measurement produced $\xi = 1.18 \pm 0.15 \pm 0.06$ as part of a multi-parameter fit to a data set that included both leptonic and hadronic tau decays.

6.2 Conclusion

Although this result is not as competitive as previous ξ parameter measurements, it provides a complimentary analysis from an independent data set. The fit returns a measurement of $|\xi| = 0.79^{+0.28+0.05}_{-0.44-0.11}$ which is consistent with Standard Model charged weak predictions and the measurement $|P_\tau| = 0.276^{+0.35+0.057}_{-0.10-0.038}$ which is consistent with Standard Model neutral weak interaction expectations. Use of previous results from SLD allow us to fix the sign of P_τ as negative causing ξ to be positive.

There is some scope for improvement in this analysis of the structure of charged weak tau decays. Some areas in which improvements may be made are as follows:

Firstly, all of the correlated tau decay measurements are limited by the statistical size of the data sets involved. Obviously this difficulty can only be cured by continued data taking. The statistical error quoted includes the errors arising from the finite size of the Monte Carlo sets used. Utilising additional Monte Carlo events may reduce this error somewhat.

Secondly, this analysis might be improved by a closer examination of the selection algorithms employed. A reduction of the background would certainly reduce systematic

errors and may improve sensitivity. The addition of the correlated ee and $\mu\mu$ tau decays would approximately double the statistical size. Developing a set of selection criteria that could allow the inclusion of these events would greatly improve the size of the statistical sample. However, this would require a good understanding of the non-tau backgrounds to which these channels are sensitive.

Finally, it is noted that a number of different fitting methods have been employed to produce Michel parameter results. Our analysis has utilised a χ^2 approach to facilitate the use of Monte Carlo events for construction of the theoretical distributions. Introducing a binned likelihood method or possibly an event by event likelihood approach might improve sensitivity in the leptonic decay channels and reduce reliance on Monte Carlo events.

In conclusion, the values of ξ and P_τ have been measured and found consistent with the Standard Model predictions.

Bibliography

[1] C. Ellis and W. Wooster, Proc. Roy. Soc.(London) **a117** (1927), 109.

[2] W. Pauli, Handbuch der Physik **24**(1933), 1.

[3] E. Fermi, Z. Phys. **88**(1934), 161.

[4] P. Renton, *Electroweak Interactions*, (Cambridge University Press, Cambridge, 1990), 570.

[5] C. Anderson, Science **76**(1932), 238.

[6] J. Street and E. Stevenson, Phys. Rev **52**(1937), 1003.

[7] S. Neddermeyer and C. Anderson, Phys. Rev **51**(1937), 884.

[8] H. Yukawa, Proc. Phys. Math. Soc. Japan **17**(1935), 48.

[9] M. Conversi *et al.*, Phys. Rev **71**(1947), 209.

[10] C. Lattes *et al.*, Nature(London) **159**(1947), 694.

[11] J. Steinberger, Phys. Rev.**74**(1948), 500.

[12] F. Reines and C. Cowan, Phys. Rev. **92**(1953), 8301.

[13] R. Davis *et al.*, Bull. Am. Phys. Soc.

[14] G. Danby *et al.*, Phys. Rev. Lett. **9**(1962), 36.

[15] R. Bolton *et al.*, Phys. Rev. **D38**(1988), 2077.

[16] T. Lee and C. Yang, Phys. Rev. **104**(1956), 254.

[17] C. Wu *et al.*, Phys. Rev. **105**(1957), 1413. **4**(1959), 217.

[18] W. Fetscher *et al.*, Phys. Lett. **B173** (1986), 102.

[19] R. Engfer and H. Walter, Ann. Rev. Part. Sci. **36**(1986), 327.

[20] C. Quigg, *Gauge Theories of the Strong, Weak, and Electromagnetic Interactions*, (Benjamin/Cummings Publishing Company, Califonia, 1983).

[21] S. Glashow, Nucl. Phys. **22**(1961), 579;
S. Weinberg, Phys. Rev. Lett. **19**(1967), 1264;
A. Salam, *Elementary Particle Theory*, ed. N. Svartholm (Almquist and Wiksells, Stockholm, 1968), 367.

[22] F. Hasert *et al.*, Phys. Lett **B46**(1973), 138.

[23] G. Arnison *et al.*, Phys. Lett. **B122**(1983), 103.

[24] G. Banner *et al.*, Phys. Lett. **B122**(1983), 476.

[25] M. Perl *et al.*, Phys. Rev. Lett. **35**(1975), 1489.

[26] S. Derenzo, Phys. Rev. **181**(1969), 1854.

[27] H. Burkard *et al.*, Phys. Lett. **B160**(1985), 343.

[28] I. Beltrami *et al.*, Phys. Lett. **B194**(1987), 326.

[29] A. Jodidio *et al.*, Phys. Rev. **D34**(1986), 1967.

[30] M. Beg *et al.*, Phys. Rev. Lett. **38**(1977), 1252.

[31] P. Herczeg, Phys. Rev. **D34**(1986), 3449.

[32] ARGUS Collaboration, Phys. Lett. **B316**(1993), 608.

[33] ARGUS Collaboration, Phys. Lett. **B349**(1995), 576.

[34] ALEPH Collaboration, Phys. Lett. **B346**(1995), 379.

[35] P. Privitera, Phys. Lett. **B288**(1992), 227.

[36] *Review of Particle Properties* Phys. Rev. **D 50** (1994).

[37] L. Michel, Proc. Phys. Soc. London Sect. A **63** (1950), 514.

[38] ALEPH Collaboration, Phys. Lett. **b321**(1994), 168.

[39] T. Kinoshita and A. Sirlin, Phys. Rev. **113** (1959), 1652.

[40] G. Altarelli *et al.*, Z Physics at LEP **1**(1989), 7.

[41] OPAL Collaboration, Nucl. Instrum. Meth. **A305**(1991), 305.

[42] J. Carter *et al.*, Nucl. Inst. and Meth. **A286** (1990), 99.

[43] S. Kluth and D. Ward, Private Communication.

[44] OPAL Collaboration, Z. Phys. **C66**(1995), 543.

[45] OPAL Collaboration, Z. Phys. **C53**(1992), 539.

[46] S. Jadach *et al.*, Comput. Phys. Commun. **79**(1994), 503.

[47] M. Bohm *et al.*, Nucl. Phys. **B304**(1988), 687;
F. Berends *et al.*, Nucl. Phys. **B304**(1988), 712.

[48] R. Bhattacharya *et al.*, Phys. Rev. **D15**(1977), 3267;

[49] D. Ward, Proceedings *MC91:Detector and event simulation in high energy physics*, (Amsterdam 1991), 204. J. Smith *et al.*, Phys. Rev. **D15**(1977), 3280.

[50] J. Allison *et al.*, Comp. Phys. Comm. **47**(1987), 55.

[51] F. James and M. Roos, Comp. Phys. **10**(1975), 343.

[52] M. Roney, Private Communication.

[53] SLD Collaboration, Phys. Rev. Lett **73**(1994), 25.

[54] ARGUS Collaboration, Phys. Lett. **B246**(1990), 278.

[55] MAC Collaboration, Phys. Rev. **D36**(1987), 1971.

[56] S. Behrends *et al.*, Phys. Rev. **D32**(1985), 2468.

VITA

Surname: GRAHAM Given Names: GRAHAM
Place of Birth: Ottawa, Ontario, Canada

Educational Institutions Attended:

University of Victoria	1993 to 1995
University of Western Ontario	1988 to 1993

Degrees Awarded

B.Sc. (Honours) University of Western Ontario 1993

Honours and Awards

University of Western Ontario Entrance Scholarship	1988
Huronia Trust Fund Scholarship	1988 to 1991
University of Victoria Fellowship	1993 to 1995

PARTIAL COPYRIGHT LICENSE

I hereby grant the right to lend my dissertation to users of the University of Victoria Library, and to make single copies only for such users or in response to a request from the Library of any other university, or similar institution, on its behalf or for one of its users. I further agree that permission for extensive copying of this thesis for scholarly purposes may be granted by me or a member of the University designated by me. It is understood that copying or publication of this thesis for financial gain shall not be allowed without my written permission.

Title of Dissertation:

Search for Right Handed Currents in Leptonic Tau Decays

Author: [redacted]

KEVIN GRAHAM
December 13, 1995